

POLITECNICO DI TORINO

Collegio di Ingegneria Meccanica, Aerospaziale, dell'Autoveicolo e della
Produzione

**Corso di Laurea Magistrale
in Ingegneria Meccanica**

Tesi di Laurea Magistrale

EFFECT OF AUTOCLAVE CURE TIME AND SURFACE PREPARATION ON FILM ADHESIVE BOND IN LIGHTWEIGHT MATERIAL JOINTS



Relatori

Prof. Giovanni Belingardi

Prof. Luca Goglio

Prof. Sayed Nassar

Candidata

Isotta Morfini

Aprile 2018

Acknowledgements

Dedicata alla mia famiglia, ai miei amici e a me. A chi c'è ora e a chi c'è sempre stato.

Ringrazio i miei genitori, per avermi sempre lasciato libera di scegliere. Mia mamma, che da sempre è per me un esempio di forza e determinazione, nel lavoro così come in qualsiasi altro ambito. Per avermi insegnato a dare sempre il massimo, senza avere paura di sbagliare, e che qualsiasi traguardo si raggiunge con impegno e passione. Mio papà, per avermi insegnato a superare gli ostacoli della vita con il sorriso. Mia sorella perché, nonostante i mille litigi, sappiamo di poter contare l'una sull'altra. Mia nonna, per la dolcezza e l'affetto che da sempre mi trasmette, e il resto della mia famiglia, per avermi supportata durante il percorso universitario e non solo.

Agli anni più intensi, quelli delle giornate sui libri, dello studio matto e disperato. Ma anche quelli delle amicizie più vere. Quelle che non passano mai. Quelle che si rinforzano, giorno dopo giorno. Per tutte le volte in cui per un attimo ho dubitato di aver fatto la scelta giusta e poi, invece, ho creduto in me stessa. Per aver sempre dato il massimo e preteso altrettanto e non essermi mai accontentata.

Ringrazio anche i miei professori per avermi guidata durante l'intero periodo di attività della tesi. Un ringraziamento particolare va al prof. Belingardi, per aver creduto in me sin dall'inizio rendendo possibile l'esperienza in America.

Al prof. Goglio, per essere stato presente anche oltreoceano, per la sua professionalità e la disponibilità dimostrata durante lo svolgimento del lavoro di tesi e la sua stesura.

A special acknowledgement goes to my advisor from Oakland University, prof. Nassar, for all his help and comprehension during my permanence at OU; for teaching me a lot, not only from the professional but also from the personal point of view.

Abstract

This study investigates the effect of soak time and surface roughness on the mechanical performance of single lap joints. Test joints are made of similar or dissimilar adherends (aluminum/aluminum or aluminum/magnesium alloys) that are autoclave-bonded using a commercially available film adhesive (Polyurethane PE399).

Test joints are fabricated through autoclave bonding: the process involves many parameters that are kept constant for all coupons, such as cure pressure, pressurization and depressurization rates, cure temperature and heating and cooling rates. The objective of this work is the evaluation of the effects of two parameters, namely soak time and surface roughness, on the mechanical performance of the joints. The reason of the choice of these two factors comes from the importance of their role on adhesion. Surface roughness in particular, has been object of many studies in the literature.

At first, the effect of these variables on the mechanical performance of the single lap joints is investigated by shear-tensile testing to determine joints static load transfer capacity. Secondly, a combination of mean load and dynamic amplitude, expressed as normalized ratios of respective static load transfer capacity of each test joint, are applied in order to evaluate the durability life of similar and dissimilar joints for different values of soak time and surface roughness.

Results, observations and conclusions are provided.

Sommario

Questo studio analizza gli effetti del tempo di cura in autoclave e della rugosità superficiale sul comportamento meccanico di single lap joint. I giunti sono realizzati con aderendi in materiale simile o dissimile (alluminio/alluminio o alluminio/magnesio) e il legame con l'adesivo in poliuretano (PE399) è ottenuto tramite un processo in autoclave.

Il processo di cura in autoclave è caratterizzato da parametri che sono costanti per tutti i provini: pressione, velocità di pressurizzazione e depressurizzazione, temperatura e velocità di raffreddamento e riscaldamento. Le due variabili oggetto di tale studio, tempo di cura e rugosità superficiale dell'area di adesione, sono due fattori che rivestono un ruolo di primaria importanza sulla forza di adesione all'interfaccia aderendo-adesivo. I loro effetti vengono studiati facendo variare il valore del tempo di cura all'interno dei limiti previsti dal produttore dell'adesivo, e conferendo due livelli di rugosità tramite operazioni di levigatura con carta vetro.

Inizialmente è analizzato l'effetto di tali parametri sul comportamento meccanico dei giunti sotto sforzo statico di tensione, per definirne il carico di rottura.

In secondo luogo viene applicato uno sforzo ciclico, combinazione di sforzo medio e variabile, entrambi normalizzati sui valori dei rispettivi carichi di rottura, per valutare la vita a fatica dei giunti a seconda delle loro caratteristiche in termini di tempo di cura e rugosità superficiale.

Infine sono presentati i risultati, le osservazioni e le conclusioni.

Table of contents

Acknowledgements	2
Abstract	3
Sommario.....	4
Table of contents	5
List of figures.....	8
List of tables	12
Chapter 1	14
Introduction	14
Adhesive bonding in automotive field	14
Single lap joints	22
Aluminum alloys in automotive field	23
Magnesium alloys in automotive field	24
Chapter 2	26
Literature survey.....	26
Chapter 3	32
Experimental setup	32

Material properties	32
Surface preparation and roughness measurement.....	35
Autoclave process control of film adhesive bonding of test joints.....	40
Chapter 4	45
Static tensile shear testing and data analysis.....	45
Design of experiment.....	45
LTC and shear-tensile tests	46
Statistical analysis of the SLJ LTC.....	50
Failure mode and SEM inspection.....	56
Chapter 5	61
Cyclic tensile-shear testing and data analysis	61
Durability tests setup	62
Test results of durability tests at low amplitude	65
Statistical analysis of the durability life of SLJs tested at low amplitude.....	68
Test results of durability tests at high amplitude	71
Statistical analysis of the durability life of SLJs tested at high amplitude	74
S-N curves	78

Failure mode and SEM inspection.....	80
Aluminum-aluminum SLJ	80
Aluminum-magnesium SLJ	82
Conclusion	88
Future work	90
References	91

List of figures

Figure 1 Methods for fuel consumption reduction	15
Figure 2 Fuel consumption related to vehicle mass	16
Figure 3 Adhesive and cohesive forces within a joint [7]	18
Figure 4 Theories of adhesion	20
Figure 5 Adhesive joints configurations [13]	23
Figure 6 SLJ configuration	23
Figure 7 Average surface roughness of the adherends after sand-paper grinding	36
Figure 8 Surface Ra for lower roughness of Al adherend	37
Figure 9 Surface Ra for higher roughness of Al adherend	38
Figure 10 Surface Ra for lower roughness of Mg adherend	38
Figure 11 Surface Ra for higher roughness of Mg adherend	39
Figure 12 SLJs preparation	40
Figure 13 SLJs disposition prior to autoclave cycle	41
Figure 14 McGill AirPressure autoclave	42
Figure 15 McGill Autoclave setup	43
Figure 16 Temperature profile during autoclave process	44

Figure 17 Pressure profile during autoclave process	44
Figure 18 DOE for static analysis of LTC	45
Figure 19 MTS Hydraulic tensile test machine	46
Figure 20 LTC of Al-Al SLJ	47
Figure 21 LTC of Al-Mg SLJ	48
Figure 22 Average LTC of SLJs with relative scatter	48
Figure 23 Load vs displacement	49
Figure 24 Pareto Chart for LTC of SLJ	50
Figure 25 Pareto Chart for LTC of Al-Al SLJ.....	51
Figure 26 Pareto Chart for LTC of Al-Mg SLJ.....	52
Figure 27 Main effects plot for LTC of Al-Al SLJ.....	53
Figure 28 Main effects plot for LTC of Al-Mg SLJ.....	53
Figure 29 Interfacial failure in Al-Mg SLJs	56
Figure 30 INCA Scanning Electron Microscope	57
Figure 31 SEM analysis of Al-Al R2 Δ T1 SLJ (1000x)	58
Figure 32 SEM analysis of Al-Mg R2 Δ T1 SLJ (250x)	59
Figure 33 Cyclic load vs time	62

Figure 34 Durability life of Al-Al SLJ tested at low amplitude.....	66
Figure 35 Durability life of Al-Mg SLJ tested at low amplitude	67
Figure 36 Pareto Chart for durability life of Al-Al SLJ tested at low amplitude	68
Figure 37 Pareto Chart for durability life of Al-Mg SLJ tested at low amplitude	68
Figure 38 Main effects plot for durability life of Al-Al SLJ tested at low amplitude	69
Figure 39 Main effects plot for durability life of Al-Mg SLJ tested at low amplitude	70
Figure 40 Durability life of Al-Al SLJ tested at high amplitude	72
Figure 41 Durability life of Al-Mg SLJ tested at high amplitude	73
Figure 42 Pareto Chart for durability life of Al-Al SLJ tested at high amplitude	74
Figure 43 Main effects plot for durability life of Al-Al SLJ tested at high amplitude	75
Figure 44 Pareto Chart for durability life of Al-Mg SLJ tested at high amplitude	75
Figure 45 Main effects plot for durability life of Al-Mg SLJ tested at high amplitude	75
Figure 46 Pareto Chart for durability life of Al-Al and Al-Mg SLJ tested at high amplitude.....	76
Figure 47 Main effects plot for durability life of Al-Al and Al-Mg SLJ tested at high amplitude.....	77
Figure 48 S-N curve of SLJs cured at $\Delta T1$	78
Figure 49 S-N curve of SLJs cured at $\Delta T2$	79
Figure 50 SEM analysis of Al-Al SLJ R1 (1000x) adhesive side	81

Figure 51 SEM analysis of Al-Mg SLJ R1 (200x) Al side 82

Figure 52 SEM analysis of Al-Mg SLJ R1 (3000x) Al side 83

Figure 53 SEM analysis of Al-Mg SLJ R1 (1500x) Al side 84

Figure 54 SEM analysis of Al-Mg SLJ R1 (1500x) Al side 84

Figure 55 SEM analysis of Al-Mg SLJ R1 (250x) Mg side 85

List of tables

Table 1 Automotive applications of magnesium alloys.....	24
Table 2 Aluminum alloy T6061-T6511 chemical composition.....	32
Table 3 Magnesium alloy AZ31B-H24 chemical composition [22]	33
Table 4 Mechanical and physical properties of the alloys.....	33
Table 5 Physical properties of PE399	34
Table 6 Autoclave cycle parameters	42
Table 7 Autoclave cycle parameters: soak time.....	43
Table 8 LTC data comparison	54
Table 9 Spectrum 1 of figure 31	59
Table 10 Spectrum 1 of figure 32	60
Table 11 Fatigue cycle parameters at low amplitude	63
Table 12 Fatigue cycle parameters at high amplitude	64
Table 13 Durability life of Al-Al SLJ tested at low amplitude.....	65
Table 14 Durability life of Al-Mg SLJ tested at low amplitude.....	66
Table 15 Durability life of Al-Al SLJ tested at high amplitude.....	72

Table 16 Durability life of Al-Mg SLJ tested at high amplitude.....	73
Table 17 Spectrum 1 of figure 50.....	81
Table 18 Spectrum 1 of figure 52.....	83
Table 19 Spectrum 1 and spectrum 2 of figures 53 and 54.....	84
Table 20 Spectrum 1 of figure 55.....	86

Chapter 1

Introduction

Adhesive bonding in automotive field

The process of adhesive bonding is one of the key joining technologies used to permanently join surfaces of similar or dissimilar materials. It finds applications in lots of sectors: not only automotive and aerospace industry, but also structural, biomedical and microelectronics applications. [1]

The most common and ancient applications of adhesives refer to building and constructions, but also woodworking, paper bonding and packaging applications.

In the medical field cyanoacrylate adhesives are used to close skin wounds, other adhesives are employed in vascular and heart surgery, in dentistry operations as filling materials, and also to ensure continuous drug dosage through transdermal patch.

The most common market applications in electronic field consist of cell phones, passport chips, where electrically conductive adhesives are usually epoxy resins containing ionic contaminants.

Adhesive bonding is more and more common in the automotive field because of the necessity to bond together dissimilar materials and because of the requirements of reducing the weight of vehicles in order to satisfy the regulations for fuel consumption and emissions. The demand for lower emissions and the necessity to improve fuel economy in passenger vehicles are the driving forces behind the increasing request for lightweight materials in the automotive field. [2]

Nearly one third of US carbon pollution comes from the transportation system: fuel economy can be improved by using lightweight materials instead of steel and this is the reason why in the last

25 years different advanced materials have been introduced into the mass-production of passenger cars. [3]

A 10% of weight reduction in a vehicle can lead to a 3.5% of fuel consumption decrease: that is why the vehicles weight reduction has become more and more interesting. Fuel consumption can be improved by reducing tyres rolling resistance, improving the vehicle aerodynamics, lightening the vehicle, and increasing its powertrain efficiency, as it is shown in Figure 1. [4]

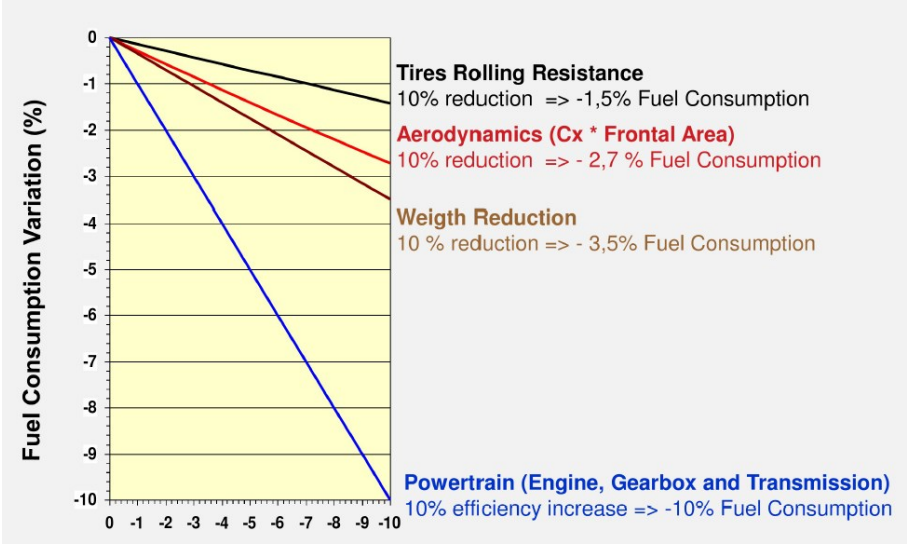


Figure 1 Methods for fuel consumption reduction

Figure 2 illustrates how fuel consumption decreases when the vehicle mass is lowered. [2]

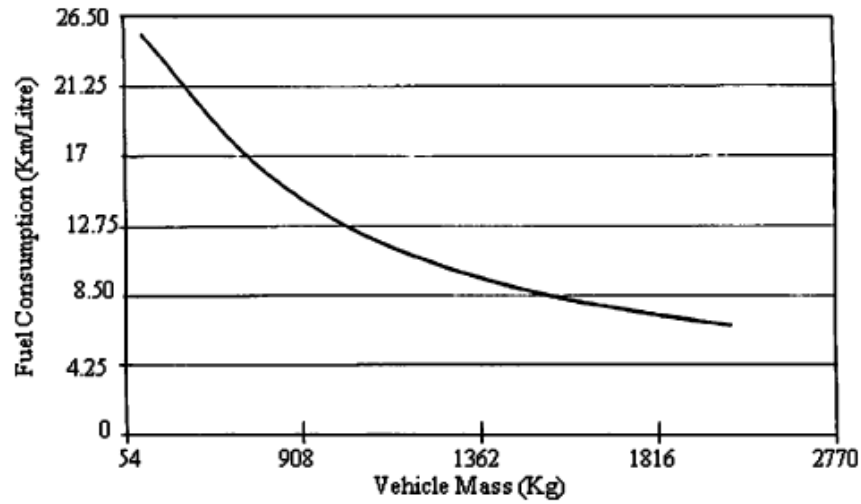


Figure 2 Fuel consumption related to vehicle mass

As already said, fuel consumption is an important issue because of the stricter regulations on vehicles emissions, that come from the necessity of reducing the green-house gases: the present regulation adopted for EU passenger cars states that the fleet average to be achieved is 130 g CO₂/km, while from 2020 this number will be reduced to 95 g CO₂/km, and to 68-78 g CO₂/km by 2025. [4]

Adhesive bonding applications

Adhesive bonding refers to the process of joining together two or more solid parts (adherends) with an adhesive, commonly a natural or synthetic polymer.

Nowadays adhesive bonding finds application in lots of different fields:

- Automotive industry
- Constructions
- Electronics
- Telecommunications
- Furniture manufacture
- Medical devices and surgery
- Textile industry

Even if the interest in adhesion can be traced back to the 1930s, there is not a complete and univocal definition of adhesion, because it is a multi-disciplinary topic that involves mechanics, thermodynamics and chemistry. [1]

Here it is reported the definition proposed by Wu. [5]

“Adhesion refers to the state in which two dissimilar bodies are held together by intimate interfacial contact such that mechanical force or work can be transferred across the interface. The interfacial forces holding the two phases together may arise from van der Waals forces, chemical bonding, or electrostatic attraction. Mechanical strength of the system is determined

not only by the interfacial forces, but also by the mechanical properties of the interfacial zone and the two bulk phases."

Theories of adhesion

In order to analyze the mechanical performance of adhesive joints it is important to understand the type of bonding that is established between adherends and adhesive.

The main forces that are present into adhesives are of two types: adhesive and cohesive.

Adhesive forces consist of molecular interactions between the substrate surface and the adhesive, while cohesion is defined as the internal strength of an adhesive as a result of a variety of interactions within the adhesive. [6]

Figure 3 shows the difference between adhesion and cohesive force at the interface between adherend and adhesive.

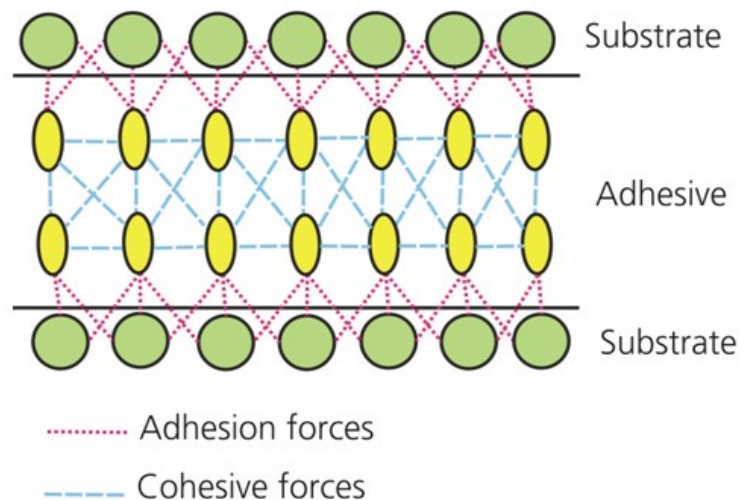


Figure 3 Adhesive and cohesive forces within a joint [7]

Lots of theories of adhesion have been developed: among them the chemical bonding (Figure 4.b) is the oldest and the most known theory. According to this theory the bond is related to chemical grouping between the surfaces of the adherend and the adhesive, and its strength is proportional to the number and type of bonds. Chemical bonds involve van der Waals forces, covalent and hydrogen bonds, and acid-base interactions. [8]

The durability of the joint is then related to the chemical characteristics of the surface.

Besides this theory, the physical bonding theory recalls the electrostatic (Figure 4.a) and the absorption theory: according to the first one the two surfaces in contact are electrostatically charged and a double layer of ions is established at their interface, and this is proved by the observation that an electrical discharge occurs when the adhesive is peeled. [9]

According to the absorption theory, a successful bond is obtained when the adhesive wets the adherend surface.

In addition to these theories, the mechanical bonding theory makes reference to interlock. Mechanical interlocking (Figure 4.d) is said to provide a weaker bond than the chemical one; it is mainly attributed to liquid adhesives (not of our interest in this study) that penetrate between two adherends and in particular into their surfaces cavities and pores. Surface roughness is an important factor since it lets the polymer penetrate into the metal surface craters and pores, enhancing the bond strength. [10]

The last type of adhesion theory involves diffusion (Figure 4.c): it states that adhesion is obtained through the inter-diffusion of molecules in between the adhesive and the adherend; since it is

applicable to long chain molecules capable of movement, it is mainly applicable when both adherend and adhesive are polymers. [8]

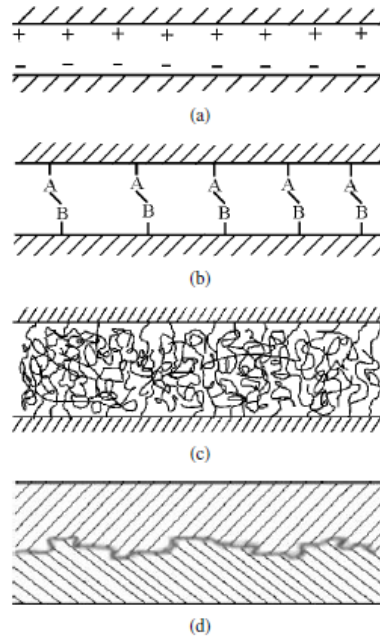


Figure 4 Theories of adhesion

Another common classification of adhesive bonding refers to structural and nonstructural adhesives: the former are referred to applications where the adherends may be subjected to high loads, while the latter are usually not subjected to significant loads but their main application is for lightweight materials. [7]

Adhesive bonding advantages and disadvantages

Adhesive bonding plays a very important role in the fastening of materials since it provides a large number of advantages over conventional bonding technologies, as stated by Ebnesajjad and Landrock [8]:

- The ability to join dissimilar materials; e.g. metallic and non-metallic
- The ability to join thin sheet materials of any shape and irregularly shaped surface, with a high design flexibility
- They provide a uniform stress distribution in the joint, that contributes to increase its fatigue resistance
- They minimize galvanic corrosion between dissimilar materials
- They are often the most convenient and cost effective fastening solution
- The operation can be almost entirely automated, and the robotic assembly techniques are the most suitable for vehicle manufacturing industries
- They do not cause change in the parts dimensions

At the same time, adhesive joints require adequate surface preparation and curing process to have long service life in very severe and hostile environments. Their mechanical behavior is geometry and load dependent and the environmental conditions can affect their properties; moreover, if compared to conventional fastening techniques, their upper service temperatures is lower. [11]

Surface pretreatment

Surface treatments are used to improve the bonding properties of the adherend and to achieve a strong bond between adherend and adhesive.

The aim of surface treatment, that includes surface preparation, surface pretreatment and surface post-treatment, is to obtain a substrate surface with good wetting properties, capable to form intermolecular and chemical interactions with the adhesive molecules, in order to increase the long-term stability of the bonded joint.

Surface preparation includes cleaning (degreasing) and preparation of the substrate surface. All the mechanical processes, such as grinding and jet-cleaning, are part of surface treatment. Together with chemical and physical processes, they alter the substrate surface structure and its chemical composition. Post treatment is made to preserve the treated surface: e.g. the application of a primer. [12]

Single lap joints

The aim of this study is to evaluate the effects of some factors on the mechanical performances of single lap adhesive joints made of aluminum and magnesium alloys, joined together through a polyurethane film adhesive: the effect of surface roughness, adherend material and soak time of the autoclave process are analyzed and two levels per factor have been taken into account.

A list of typical configurations of adhesive joints is presented below in Figure 5: the one we are focusing on in our study is the SLJ in Figure 6.

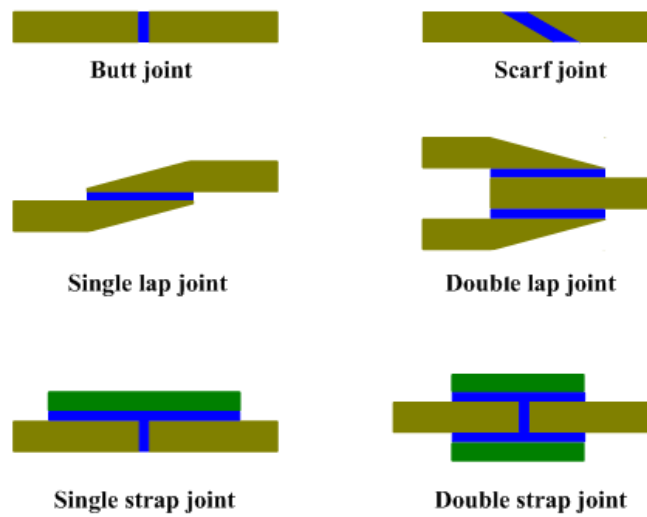


Figure 5 Adhesive joints configurations [13]

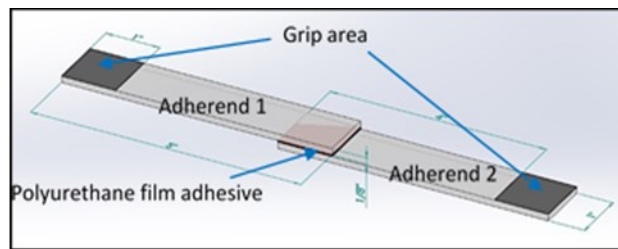


Figure 6 SLJ configuration

Aluminum alloys in automotive field

Aluminum alloys are characterized by a relatively low density (2.7 g/cm^3 as compared to 7.9 g/cm^3 for steel), and among their advantage we find high electrical and thermal conductivities and resistance to corrosion in the ambient atmosphere. They find applications in aircraft structural parts, beverage cans, bus bodies and in automotive parts, such as engine blocks, pistons and manifolds. They are widely used for automobile bodies because their higher strength to weight ratio, with respect to steels, makes them more interesting from the fuel efficiency point of view. Moreover they have higher stretch formability than steels with comparable strength levels. [13]

Magnesium alloys in automotive field

Magnesium and its alloys have more and more widespread as automotive applications since it is the lightest of all the engineering materials, with a density of 1.74 g/cm^3 . By using magnesium alloys it is possible to save up to 70% of automotive components weight. Its use in this field is inferior if compared to aluminum alloys because of its higher cost. Anyway in the recent years, new technologies and productive processes have allowed more competitive prices. More ductility, good castability and better noise and vibration dampening than aluminum are its main advantages besides its specific strength and its weight. [2]

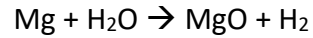
In Table 1 the main automotive applications of magnesium alloys are listed.

Table 1 Automotive applications of magnesium alloys

Engine and parts	Transmission	Interior parts	Chassis components	Body components
Engine block		Steering wheel cores	Rod wheels	Cast components,
Gear box		Seat components	Suspension arms	Inner bolt lid section
Intake manifold		Instrument panel	Engine cradle	Cast door inner
Crankcase		Steering column components	Rear support	Radiator support
Cylinder head cover		Brake and clutch pedal	Tailgate (AM50)	Sheet compo
Oil pump housing		Air bag retainer		Extruded components
Oil pump		Door inner (AM50)		
Transfer case				
Support (AZ91D)				
cover (AZ91D)				
Cam				
Bedplate				
Engine block (Ford)				
Oil pan (Ford)				
Front cover (Ford)				
Engine cradle (Ford)				

Among the main technological barriers that limit the usage of magnesium alloys for automotive applications, in comparison with aluminum alloys, its high reactivity, inferior corrosion and creep resistance and galvanic corrosion can be mentioned.

The most common reactions of magnesium are the oxidation with water and the hydroxide reaction, respectively:



These reactions can occur at room temperature: magnesium alloy behaves as a corroding anode with the metallic component in its proximity; their consequences are the reduction of the salvage value of the alloy and the increase of fire risk. That is why protective finishes, anodic coatings or paint are used.

Being magnesium at the bottom of the galvanic series, the percentage of heavy metals impurities must be reduced (Fe, Ni and Cu) to prevent from galvanic corrosion.

Chapter 2

Literature survey

This work aims at analyzing the effect of the adherends' surface roughness and autoclave cure time on the durability life of SLJs.

In the literature there are a few studies that take into account the influence of surface roughness on the strength of the adhesion between metallic alloy adherend and a film adhesive. Not only the surface roughness, but also the curing time during the autoclave process of baking the joints is one of the factors whose effects have been analyzed.

Most of the past studies about SLJs mechanical performances in tensile-shear pay attention to the water exposure and moisture influence on the degradation of the joints adhesive strength, but only a few take into consideration the effect of surface micro-roughness as a main factor, nor the effect of soak time on their static LTC.

Previous authors have studied the effect of saline environment on the mechanical properties of adhesive joints made of steel adherends and epoxy adhesive: among their main disadvantage, poor resistance to aggressive environment is one of the main restrictions for lots of applications.

[14]

Pereira et al. have observed that high temperature and water exposure decrease joint's strength, and their combination accelerates the process of degradation. This is in accordance with previous works of Banea and da Silva [15], in which temperature, humidity and moisture affect the

strength of adhesive joints and this depends mainly upon the cure shrinkage and the coefficient of thermal expansion of the adhesive.

Knox and Cowling [16] have experimentally studied the effect of aging on structural adhesives that bonded thicker surface-treated adherends in marine applications. Test specimens of steel were shot blasted and degreased with acetone before being bonded with an epoxy structural adhesive. The effect of high humidity and salt water was investigated. They found out that liquid water absorption caused the failure mode in tensile-shear tests have changed to interfacial failure, instead of cohesive failure of baseline joints prior to aging. The weakening of the adhesive strength is mainly due to diffusion through adhesive, transport along the interface and diffusion through the adherend, if permeable. The authors found out that liquid water affects the failure mode of the adhesive joints by changing it from cohesive to adhesive, since it leads to the degradation of the interface between adherend and adhesive.

Pires et al. [17] studied the stress distribution of bi-adhesive bonded lap joints, under a tensile load. Their work is about the decrease of the stress concentration at the edge of the overlap of the joint, by means of the use of different adhesives with different stiffness. In particular they adopted two different adhesives; ESP110 was the stiffer adhesive applied in the central portion of the overlap length, while DP490 was the softer adhesive, applied at the edges. The aluminum adherends were cleaned with solvent and then grit blasted, before being cured at 120°C for 1 hour and 20 minutes (compromise between the two curing cycles of the different adhesives). After a tensile test, performed with a crosshead speed of 1 mm per minute, they observed that

this option contributes to increase the joint's strength, up to 22%. A bi-adhesive bonded joint allows to lower the stress concentration, which is higher when the adhesive used is only one.

Also the work of Lucic et al. [18] takes into account the influence of the overlap length on SLJs made of aluminum A199.5 adherend and a two-component epoxy adhesive. They achieved the objective of finding the optimal overlap length that allows to increase the joint strength, through experimental and numerical simulation.

The study of Borsellino et al. [19] investigates the effects of the surface treatment and induced roughness on aluminum alloy SLJs, bonded with different types of resins (polyester, vinylester, and epoxy). Aluminum AA6082 substrates of 1.5 mm thickness were used and tested according to ASTM D1002; the surfaces were mechanically abraded through P40 and P180 grinding papers and the 2.5% of the thickness was removed. After the surface cleaning and the roughness measurement, the wettability of the substrate according to the resin and the surface profile was evaluated. The SLJs obtained were tested and then their shear strength was compared. The surface roughness influenced the resins wettability and the joint strength; the mechanical abrasion seems to be effective only until an optimal value of roughness is reached. They found no interaction between the roughness and the resin type.

If the studies about surface roughness and soak time influence on SLJ are a few, even less studies investigate the influence of the same factors on the fatigue life of SLJ.

In terms of fatigue strength of adhesive joints, Pereira et al. studied the effect of water exposure and saline solution on steel adherends bonded with an epoxy adhesive: the saline solution caused a more severe decrease in fatigue strength, up to 39% for 10^5 cycles [14].

The influence of adherend macroroughness on the durability of aluminum joints was investigated by Critchlow and Brewis [20]: they studied the effect of grit blasting on aluminum epoxide SLJs. They compared the initial joint strength to the strength after immersion in ionized water for 24, 85 and 211 days: the macroroughness of the adherends showed a significant influence on the durability of the joints. Finer grits produced more durable joints while the higher grits level produced joints whose strength showed a gradual decrease with increasing time of immersion in water.

Ferreira et al. analysed the effect of water immersion and time of exposure on the fatigue behaviour of adhesive lap joints made of composite (E-glass fibers and polypropylene adherends) and a rubber and plastic adhesive. [21]

SLJ generally have low fatigue performance since the ends of the overlap are exposed to high concentration of peel and shear stresses. Roughness is taken into account in order to correlate it with the failure mode after the fatigue test. An interfacial failure is associated to a lower roughness profile, while a cohesive failure is related to a higher roughness profile and deeper steps.

Krenk et al. [22] tested the fatigue resistance of aluminum adhesive SLJs under cyclic shear and bending load. They analysed the crack growth and its propagation through the use of non-linear finite elements models. The specimens were made of adherends in aluminium alloy 6061-T6 and adhesive epoxy 9323. They adopted Zienkiewicz et al. model [23], according to which the material model is defined by the overlapping of some elastic perfectly plastic elements, with different elastic stiffness and yield. They observed a linear behaviour of the joint under cyclic load until

before failure; in addition, the cyclic tests they performed were not dependent on the adhesive thickness, while this factor was influential in terms of static load (the higher the adhesive thickness, the higher the static load). As regards the crack growth, they did not observe a significant initiation period and they suggested an energy release rate propagation model, which reflects the independence of the cracks from the adhesive thickness.

The study of Quaresimin and Ricotta [24] is about SLJs in carbon/epoxy composite bonded with epoxy adhesive and tested under static and fatigue tensile load. They evaluated the influence of the overlap length as well as the geometry of the corner on the fatigue strength. The surface preparation of the adherends was taken into account too, for what regards the static strength. They found out that a longer overlap and a spew fillet give advantages in terms of static strength, up to 25% if compared to the squared edge joints, and that an external layer of peel-ply provides an average increase of 10% on the tensile strength of the joints. They also analysed the failure mode and the crack nucleation and growth under the fatigue cycle; in terms of fatigue life, the crack nucleation time was found to be between 20 and 70% of it, according to the stress concentration and the length of the overlap.

Pirondi and Moroni [25] predicted the fatigue failure of metal to metal adhesive joints bonded with different types of structural adhesives. They also studied the influence of the overlap length on the fatigue life of joints (the shorter the joint, the longer its life) and the crack nucleation and propagation process. The crack nucleates after a few cycles and the duration of the joint depends mainly on the propagation phase.

Hurme and Marquis [26] investigated hybrid joints that combine adhesives and bolts. They investigated fatigue damage in the bonded interfaces through scanning electron microscopy. The identification of interface failure modes concluded that a progressive damage in the adhesive and fretting fatigue are the major responsible for fatigue failure.

Test specimens from HSS sheets were grit blasted and the interfaces were bonded with a two-component structural epoxy adhesive.

The SEM analysis revealed that the fatigue failure was caused by multiple cracks, voids and inclusions: a not uniform local stress field distribution in the adhesive is due to surface roughness contour and existing voids and inclusions. Stress concentration instead of poor adhesion is the main reason for cracks formation and propagation at the interface.

In conclusion, the lack of an in-depth analysis as well as the importance of the effects of surface micro-roughness and cure time on the static strength and fatigue performance of SLJs in tensile-shear test, is the motivation for this study.

Chapter 3

Experimental setup

Material properties

In this study the mechanical behavior of SLJs made of similar or dissimilar adherends of lightweight metallic alloys and polyurethane adhesive is investigated. The adherends are rectangular blocks of aluminum and magnesium alloys, respectively 6061-T6511 and AZ31B-H24. Aluminum 6061-T6511 has been solution heat treated and artificially aged, while magnesium AZ31B-H24 has been strain-hardened.

In Table 2 and Table 3 their chemical composition are summarized; while Table 4 is referred to their mechanical and physical properties.

Table 2 Aluminum alloy T6061-T6511 chemical composition

Component	Amount (wt. %)
Aluminum	Balance
Magnesium	0.8-1.2
Silicon	0.4-0.8
Iron	Max. 0.7
Copper	0.25-0.40
Zinc	Max. 0.25
Titanium	Max. 0.15
Manganese	Max. 0.15
Chromium	0.04-0.35
Others	0.05

Table 3 Magnesium alloy AZ31B-H24 chemical composition [22]

Element	Content (%)
Magnesium	97
Aluminum	2.5-3.5
Zinc	0.6-1.4
Manganese	>=0.20
Silicon	<=0.10
Copper	<=0.050
Calcium	<=0.040
Iron	<=0.050
Nickel	<=0.050

Table 4 Mechanical and physical properties of the alloys

Material	Designation	Density	Elongation	UTS	E
		(g/cm ³)	(%)	(MPa)	(GPa)
Al alloy	6061-T6511	2.7	9-13	260-310	70-80
Mg alloy	AZ31B-H24	1.77	15	290	45

The adhesive that has been used for the purpose of realizing the SLJs is a high performance aliphatic polyether film, Krystalflex PE399. It is used for glass, polycarbonate, acrylic and CAB lamination applications.

Among its advantages there are:

- Excellent laminated transparency
- Excellent hydrolysis and microbial resistance
- Good low temperature flexibility
- Enhanced UV stability
- Medium modulus

- Excellent cold impact

In Table 5 its physical properties are presented.

Table 5 Physical properties of PE399

Property	Key	DIN	Unit	Value	ASTM	Unit	Value
Hardness	M	53505	Shore A	80	D-2240	Shore A	80
Tensile Strength	E	53504	MPa	45	D-412	psi	6500
Elongation @ break	E	53504	%	500	D-412	%	500
100% Modulus	E	53504	MPa	2	D-412	psi	300
300% Modulus	E	53504	MPa	7	D-412	psi	1000
Tear Resistance	E	53515	N/mm	37	D-624	pli	210
Specific Gravity	E	53478		1.07	D-792		1.07
Softening Range Low	E	Huntsman TMA	°C	80	Huntsman TMA	°F	175
Softening Range High	E	Huntsman TMA	°C	140	Huntsman TMA	°F	285
Midpoint Tg by DSC	E	Huntsman DSC	°C	-36	D-3418	°F	-33

E = 0.050" extruded film cut to ASTM requirements
M = Injection moulded parts to meet DIN & ASTM requirements
ASTM measurements were tested at 20 in/min.
DIN measurements were tested at 500 mm/min.

Surface preparation and roughness measurement

Surface roughness is one among the major aspects to take into account when the shear-tensile behavior of a SLJ is investigated.

In this work, the effect of the adherends surface roughness has been evaluated. To do so, the coupons surface has been abraded with sand paper: the aim of this treatment is to give two different levels of roughness to the surface that are in contact with the film adhesive.

Through different sand-papers sheets, the aluminum alloy and the magnesium alloy have been grinded for an area of 1 squared inch (25.4 mm x 25.4 mm), that corresponds to the overlap area on which adhesion takes place during autoclave process.

The sand-papers used vary from P150 and P2000, which correspond respectively to very fine macro grit level and ultra-fine micro grit. The operation of abrading the surface with sandpaper is repeated many times, until the right average value of surface roughness is reached.

In particular, the grinding has been made by hand, by moving the sand-paper perpendicularly to the main axis of symmetry of the coupon, until the evidence of previous work was canceled. In fact the coupons came from alloy sheets that have been produced by extrusion, so some straight lines were evident.

After this operation, roughness measurements have been made by using the Wyko NT1100 optical profiler [27].

Wyko NT1100 surface profiler has two different working modes: PSI and VSI. PSI stands for Phase Shifting Interferometry, and it is reliable for smooth surfaces, while VSI, that stands for Vertical

Scanning Interferometry, is appropriate for rough surfaces and deeper steps. The appropriate working mode is chosen according to the range it is suitable for: in this case, a VSI mode has been adopted, since its range is up to 1 mm of vertical depth. VSI mode is based on white light vertical scanning interferometry: light reflected from a reference mirror combines with light reflected from a sample to produce interference fringes, where the best-contrast fringe occurs at best focus. In order to get the most accurate measurement as possible, the stage tilt should be adjusted to get the fringes on the whole surface observed. In order to obtain an accurate and precise value of the surface roughness, the measurement has been repeated three times per each sample.

Then the average value has been considered: in the following figure the difference between the surface average roughness for both aluminum and magnesium samples is shown.

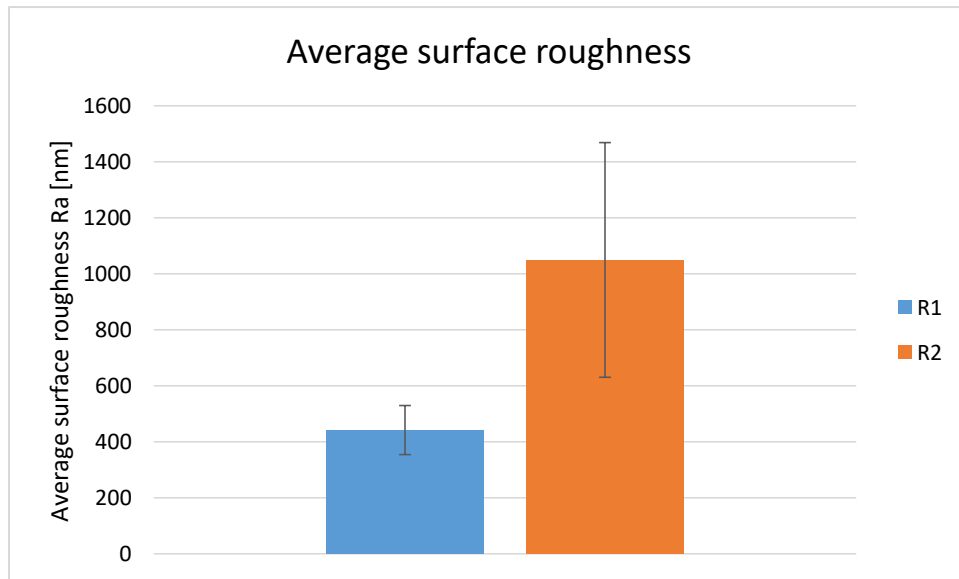


Figure 7 Average surface roughness of the adherends after sand-paper grinding

As an example, Figure 8, Figure 9, Figure 10 and Figure 11 show the surface average roughness profile of the aluminum and magnesium adherends evaluated with the WYKO NT1100.

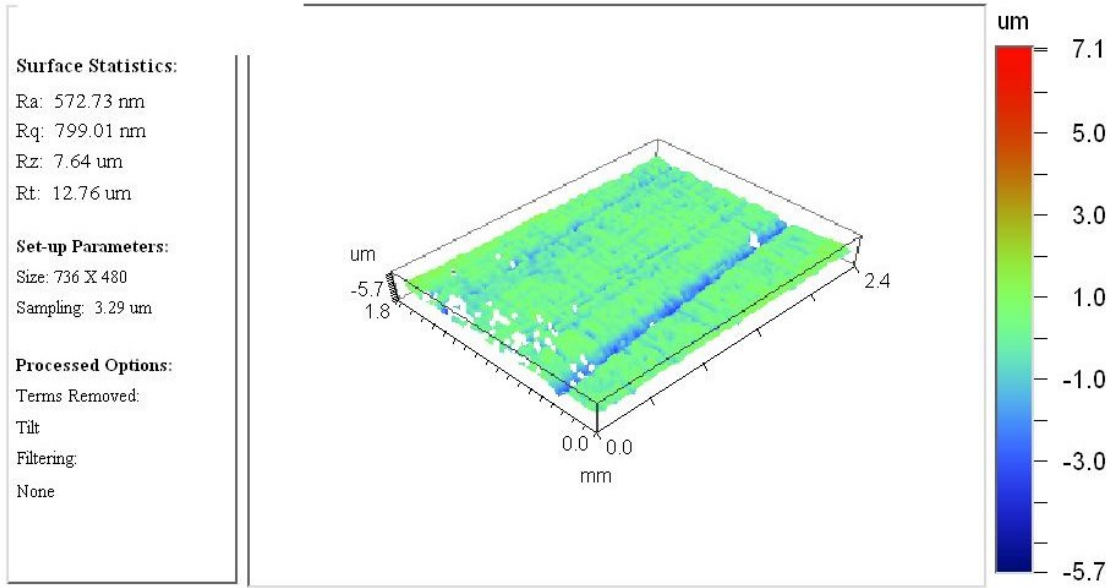


Figure 8 Surface Ra for lower roughness of Al adherend



3-Dimensional Interactive Display

Date: 11/01/2017

Time: 10:55:47

Surface Stats:

Ra: 1.10 μm

Rq: 1.42 μm

Rt: 13.24 μm

Measurement Info:

Magnification: 2.56

Measurement Mode: VSI

Sampling: 3.29 μm

Array Size: 736 X 480

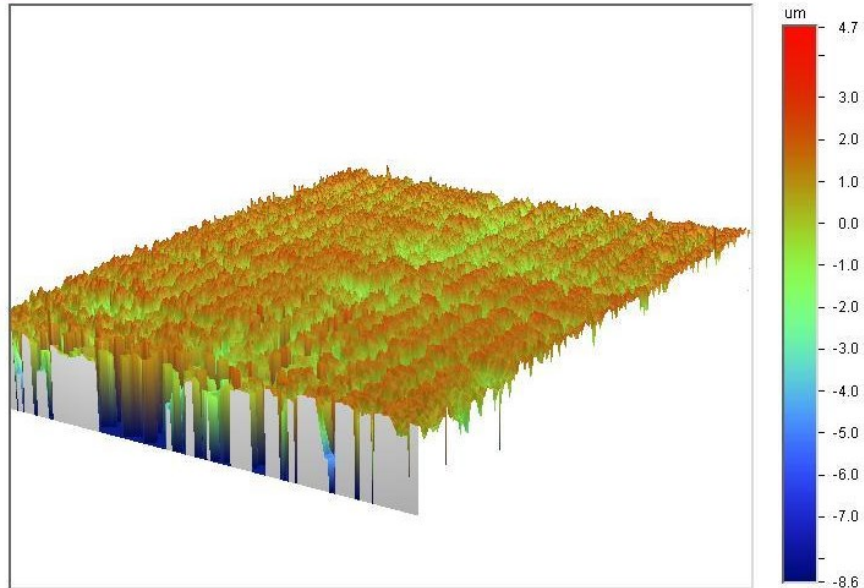


Figure 9 Surface Ra for higher roughness of Al adherend



3-Dimensional Interactive Display

Date: 11/16/2017

Time: 09:48:39

Surface Stats:

Ra: 597.91 nm

Rq: 818.17 nm

Rt: 16.37 μm

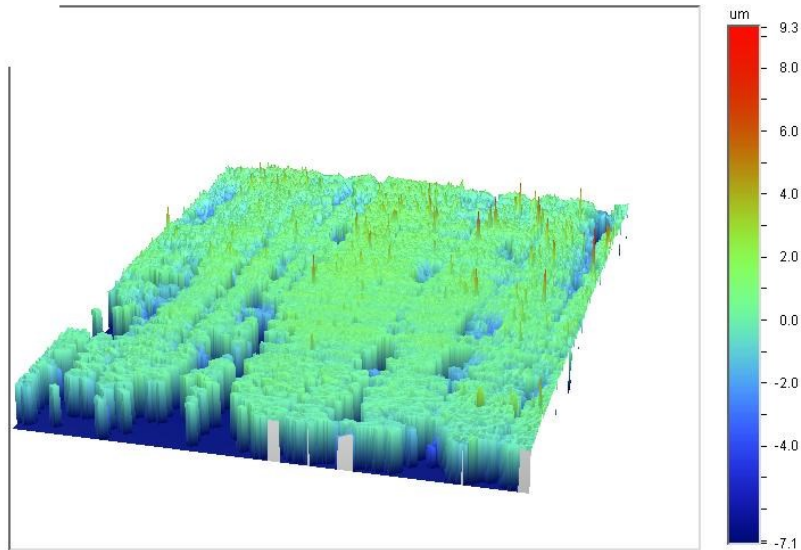
Measurement Info:

Magnification: 2.56

Measurement Mode: VSI

Sampling: 3.29 μm

Array Size: 736 X 480



Title:

Note:

Figure 10 Surface Ra for lower roughness of Mg adherend

3-Dimensional Interactive Display

Date: 11/06/2017
Time: 09:50:09

Surface Stats:

Ra: 1.16 μm
Rq: 1.54 μm
Rt: 18.17 μm

Measurement Info:

Magnification: 2.56
Measurement Mode: VSI
Sampling: 3.29 μm
Array Size: 736 X 480

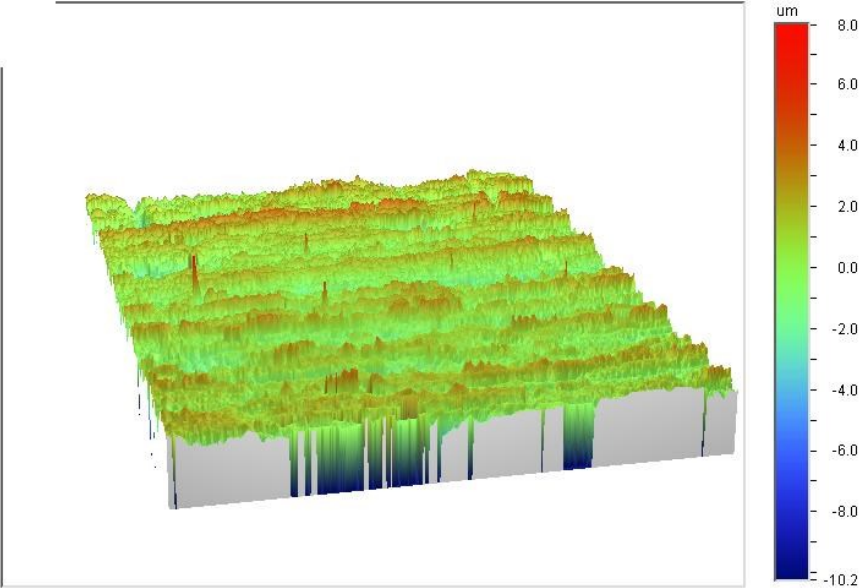


Figure 11 Surface Ra for higher roughness of Mg adherend

Autoclave process control of film adhesive bonding of test joints

To create adhesion between the adherends and the adhesive, the samples are cured in autoclave. Prior to the autoclave process, the coupons' surface has been sanded and after this operation, it has been cleaned with acetone. A clean surface is necessary in order to have a proper adhesion at the interface between adherend and adhesive.

As it is shown in Figure 12 and Figure 13, the coupons are disposed on a stainless steel tray and they are covered by different clothes and plastic layers that are used to seal them and to make possible the creation of vacuum. The two adherends are kept aligned through other tabs, made of steel, that have their same thickness.

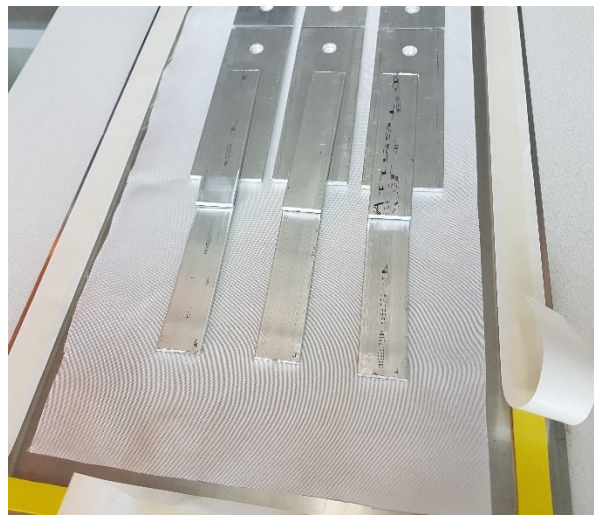


Figure 12 SLJs preparation



Figure 13 SLJs disposition prior to autoclave cycle

Vacuum is created through the vacuum pump that is connected to the tray by means of two valves and two flexible tubes. The tray is inserted in the autoclave and the vacuum is created: the sealing procedure requires high attention and precision because if the vacuum bag is not sealed properly, it may break during the autoclave cycle and it would be necessary to immediately stop the cycle.

After this operation, the setup of the cycle is controlled by using the software that regulates autoclave parameters. The autoclave door is closed by means of an electro-pneumatic pin and a pneumatic mechanism, the cooling water valve and the compressor valve are opened and the cycle is started. The autoclave, whose picture is in Figure 14, is a McGill AirPressure product; the company is located in Ohio and it designs, builds and installs a wide variety of pressure and vacuum vessels for many different industries and processes.



Figure 14 McGill AirPressure autoclave

It is possible to control all the parameters that affect the cycle inside the autoclave during the whole duration of the process: all the parameters are kept constant during the autoclave cycle, except for the soak time. A detailed description of the setup is in Table 6 and Table 7 and a screenshot of the program setup is provided in Figure 15.

Table 6 Autoclave cycle parameters

heating rate	13 F/min	13 C/min
max T	260 F	127 C
cooling rate	13 F/min	13 C/min
pressurization rate	6.25 psi/min	0.043 MPa/min
max p	125 psi	0.86 MPa
depressurization rate	6.25 psi/min	0.043 MPa/min

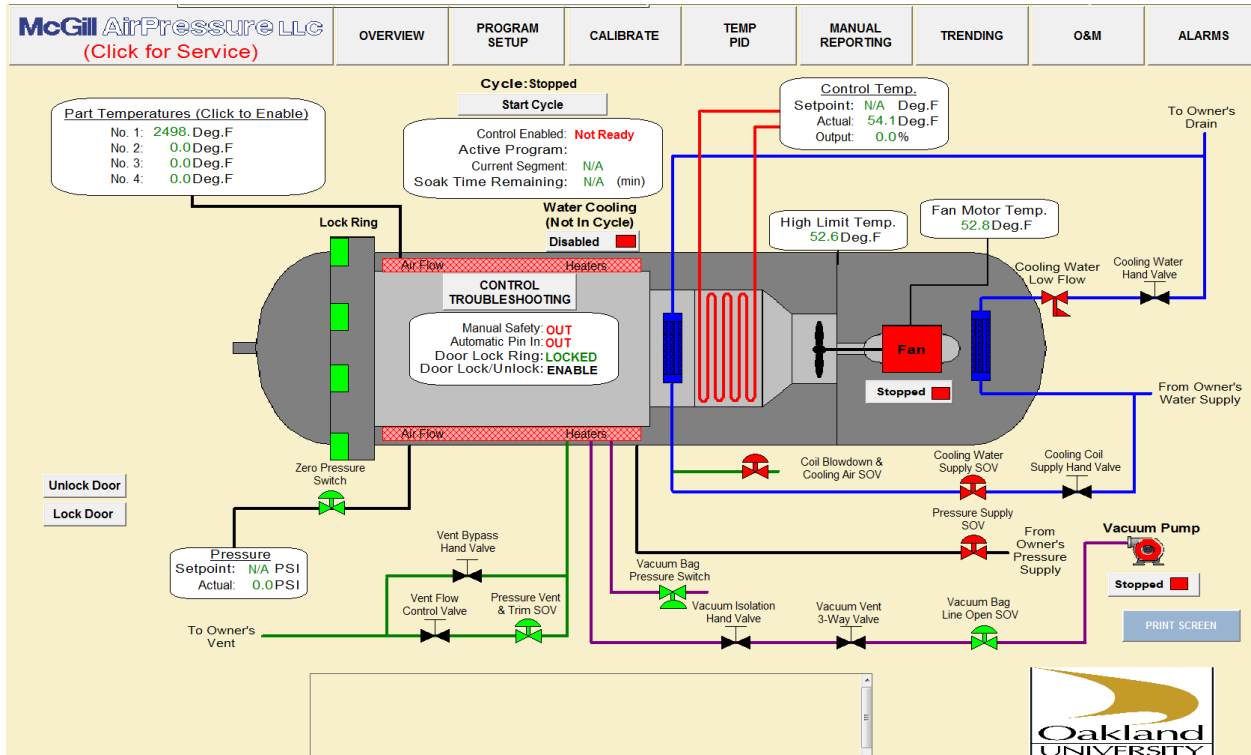


Figure 15 McGill Autoclave setup

Since soak time is one of the variable factors of the analysis of this study, two different values of soak time have been taken into account. Both the two levels fall within the range of curing time recommended by the adhesive provider.

Table 7 Autoclave cycle parameters: soak time

soak time	40 min	80 min
level	1	2

In Figure 16 and Figure 17 the two graphs show the variation of temperature and pressure during the two different autoclave cycles.

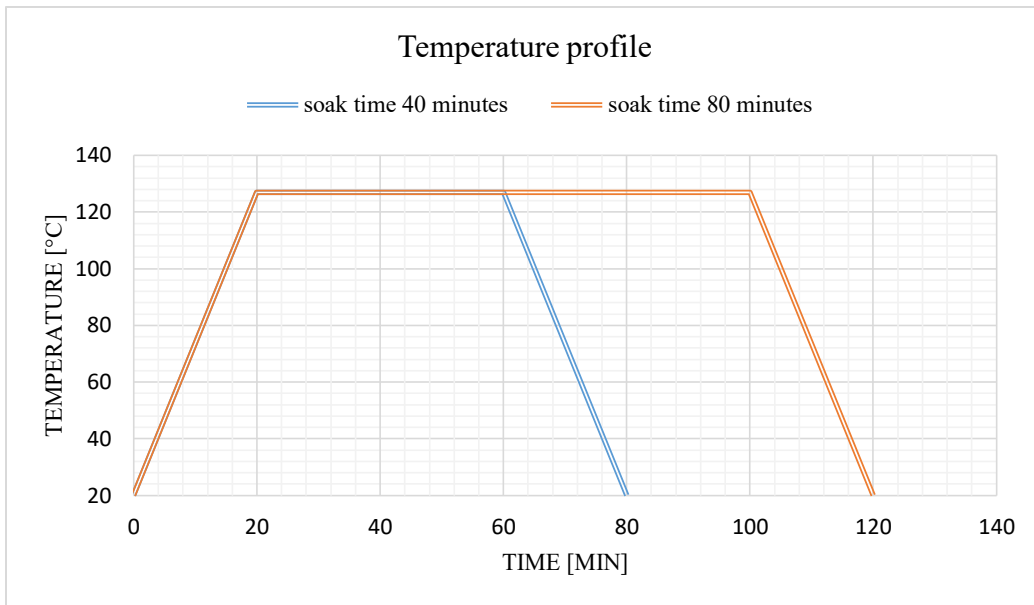


Figure 16 Temperature profile during autoclave process

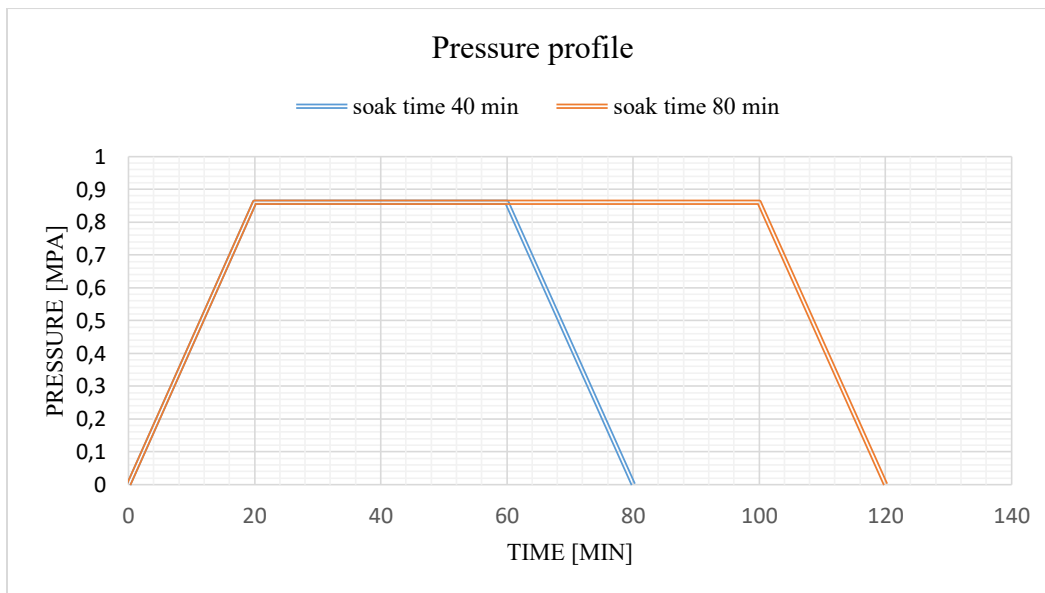


Figure 17 Pressure profile during autoclave process

Chapter 4

Static tensile shear testing and data analysis

Design of experiment

The first part of this work aims at evaluating the static LTC of the SLJs, and the objective is the analysis of the influence of surface roughness, soak time and material on the mechanical performance of the joints.

To perform a full factorial analysis of the experiment, 24 SLJs have been fabricated by means of the autoclave cycles. Six SLJs could fit in each autoclave cycle, so four autoclave cycles were necessary in order to have the proper number of joints that permit to evaluate all the considered factors.

The cycle parameters of the autoclave procedure were kept the same except for soak time: the following figure explains the design of experiment and the differences between the four cycles.

$$\left\{ \begin{array}{l} Al - Al \left\{ \begin{array}{l} R_a 1 \left\{ \begin{array}{l} \Delta t_1 \text{ Cycle 1} \\ \Delta t_2 \text{ Cycle 2} \end{array} \right. \\ R_a 2 \left\{ \begin{array}{l} \Delta t_1 \text{ Cycle 1} \\ \Delta t_2 \text{ Cycle 2} \end{array} \right. \end{array} \right. \\ \\ Al - Mg \left\{ \begin{array}{l} R_a 1 \left\{ \begin{array}{l} \Delta t_1 \text{ Cycle 3} \\ \Delta t_2 \text{ Cycle 4} \end{array} \right. \\ R_a 2 \left\{ \begin{array}{l} \Delta t_1 \text{ Cycle 3} \\ \Delta t_2 \text{ Cycle 4} \end{array} \right. \end{array} \right. \end{array} \right.$$

Figure 18 DOE for static analysis of LTC

LTC and shear-tensile tests

After every cycle, the adhesive SLJs were tested in a hydraulic tensile test machine produced by MTS and a shear-tensile test was performed.

Figure 19 provides a picture of the tensile test machine used for the LTC evaluation.

The tests were performed approximately 24 hours after the end of each autoclave cycle, in order to test all the samples under the same conditions.

Tensile tests were performed following the ASTM D1002 standard: an axial load is applied at a constant speed of 1.27 mm/min. Each end of the specimen is engaged to the grippers for 1 inch length; rectangular spacers of the same thickness as the two adherends are put in the grippers in order to reduce the bending effect during shear-tensile tests for LTC.

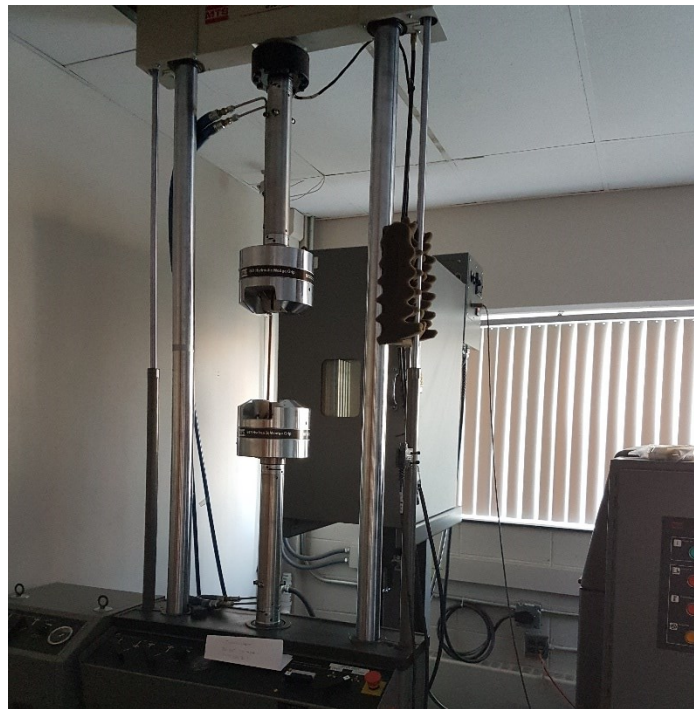


Figure 19 MTS Hydraulic tensile test machine

Data were recorded and the load vs displacement curve give information about the maximum load that each SLJ could sustain. Figure 20 and Figure 21 present the results of the ultimate tensile strength differentiated according to the adherend material, while Figure 22 shows the average results of LTC of aluminum/aluminum joints and aluminum/magnesium joints with their relative scatter.

The following chapter provides an analysis of the results obtained from these tests.

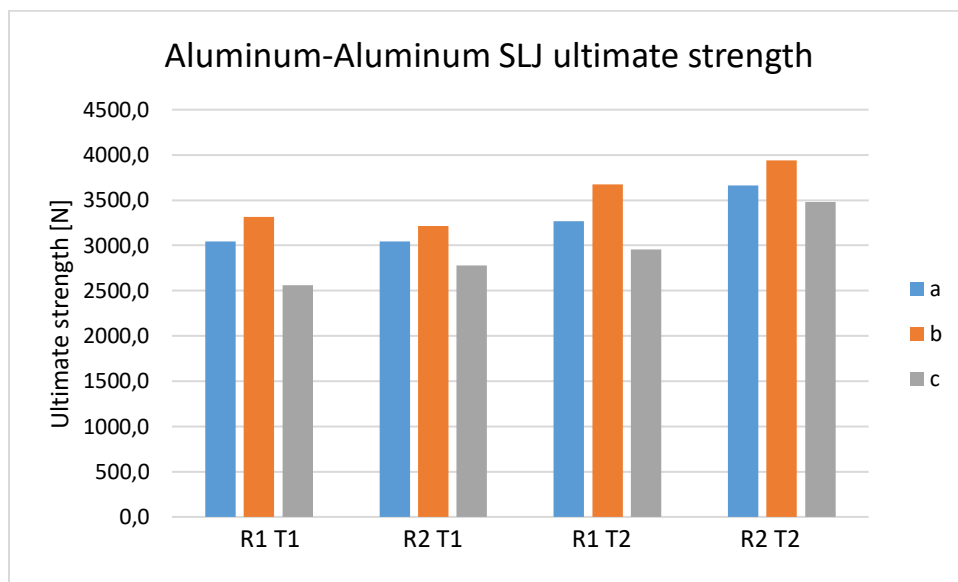


Figure 20 LTC of Al-Al SLJ

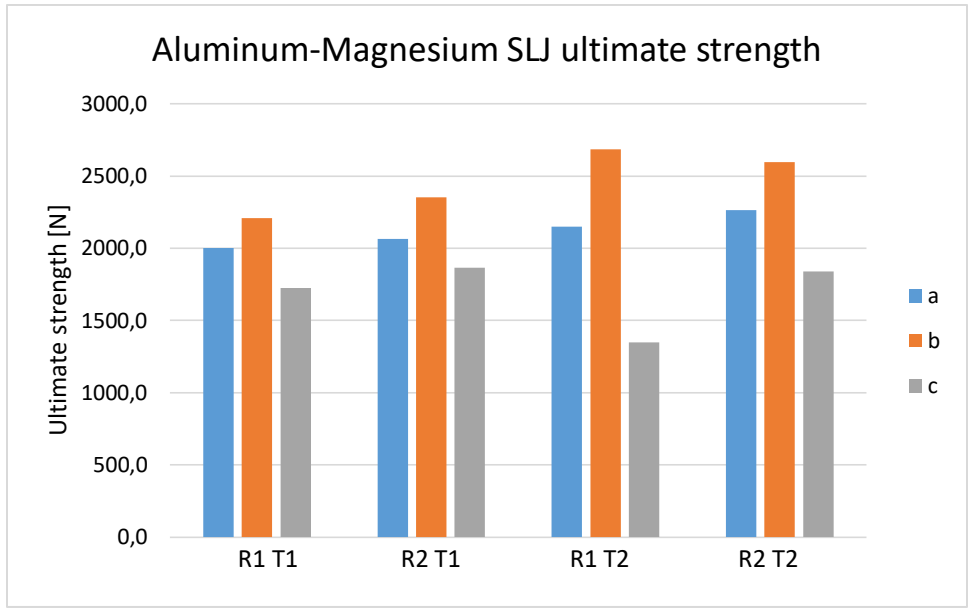


Figure 21 LTC of Al-Mg SLJ

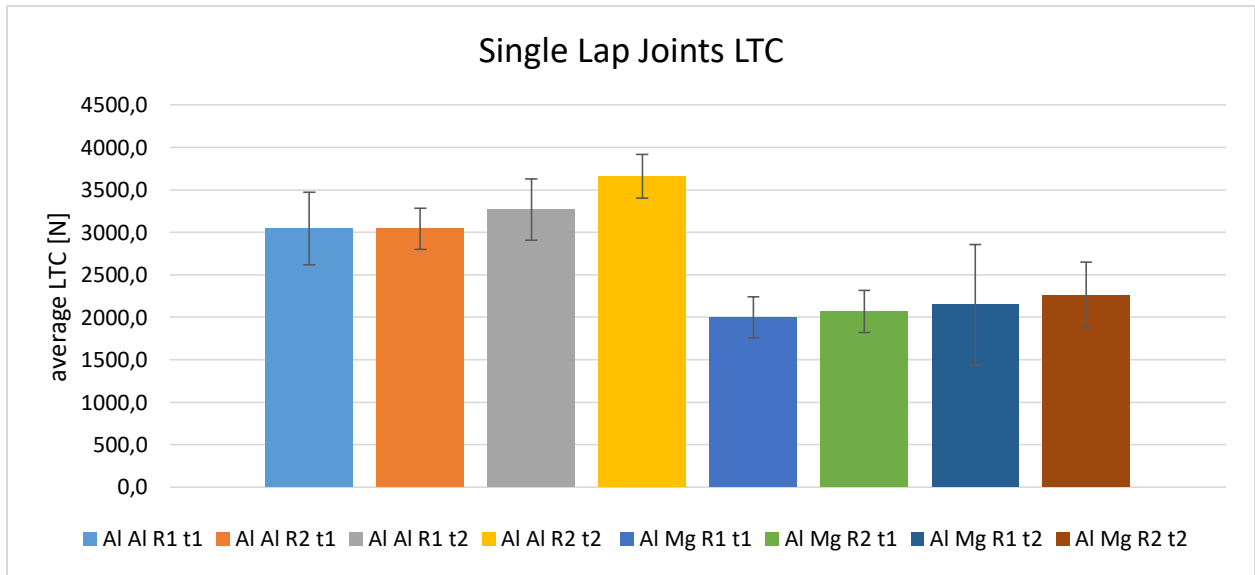


Figure 22 Average LTC of SLJs with relative scatter

As an example, the following graph in Figure 23 shows the load vs displacement curves obtained from the shear-tensile tests of some of the SLJs.

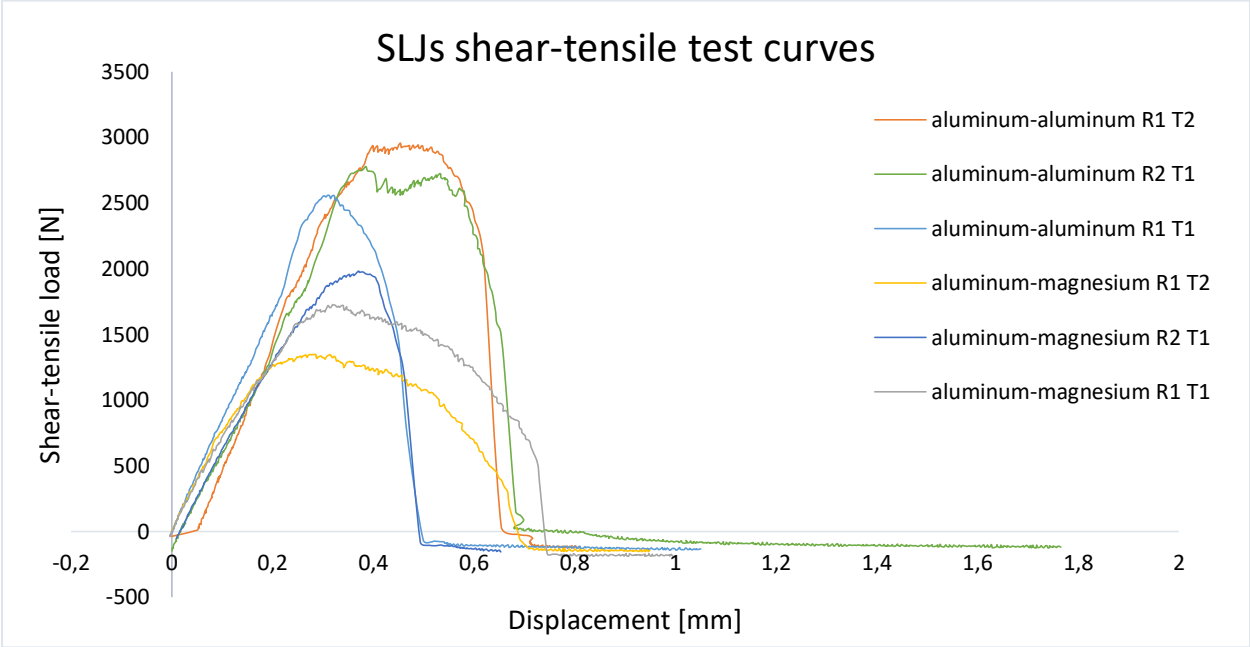


Figure 23 Load vs displacement

Statistical analysis of the SLJ LTC

A statistical analysis of the data coming from the shear-tensile tests has been performed.

The Pareto charts show which factors are significant and how they affect the response. They show the absolute values of the standardized effects from the largest effect to the smallest effect.

The standardized effects are t-statistics that test the null hypothesis that the effect is 0. A reference line indicates which effects are statistically significant.

By looking at Figure 24 it is clear that the most important factor among the three is material, followed by soak time and roughness, which are however under the significance level.

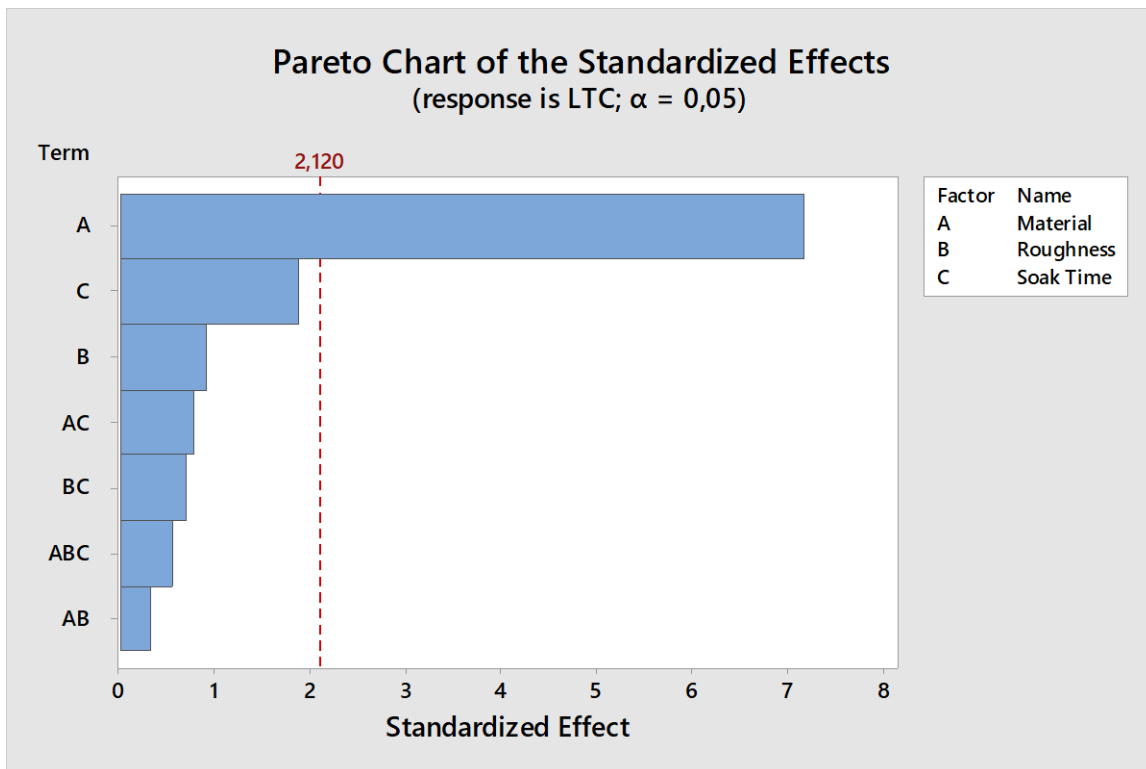


Figure 24 Pareto Chart for LTC of SLJ

Since the material that constitutes the second adherend gives the most important effect, the analysis of the same data is presented, differentiated according to the material, in Figure 25 and Figure 26. In this way, the influence of roughness and soak time is not overshadowed by that of material.

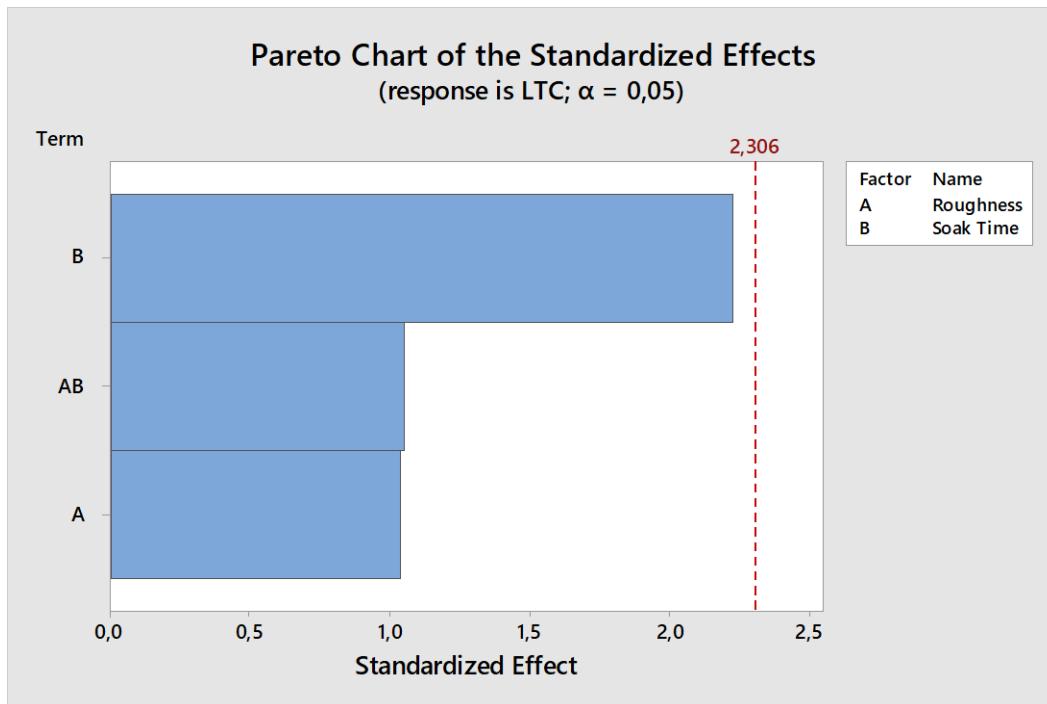


Figure 25 Pareto Chart for LTC of Al-Al SLJ

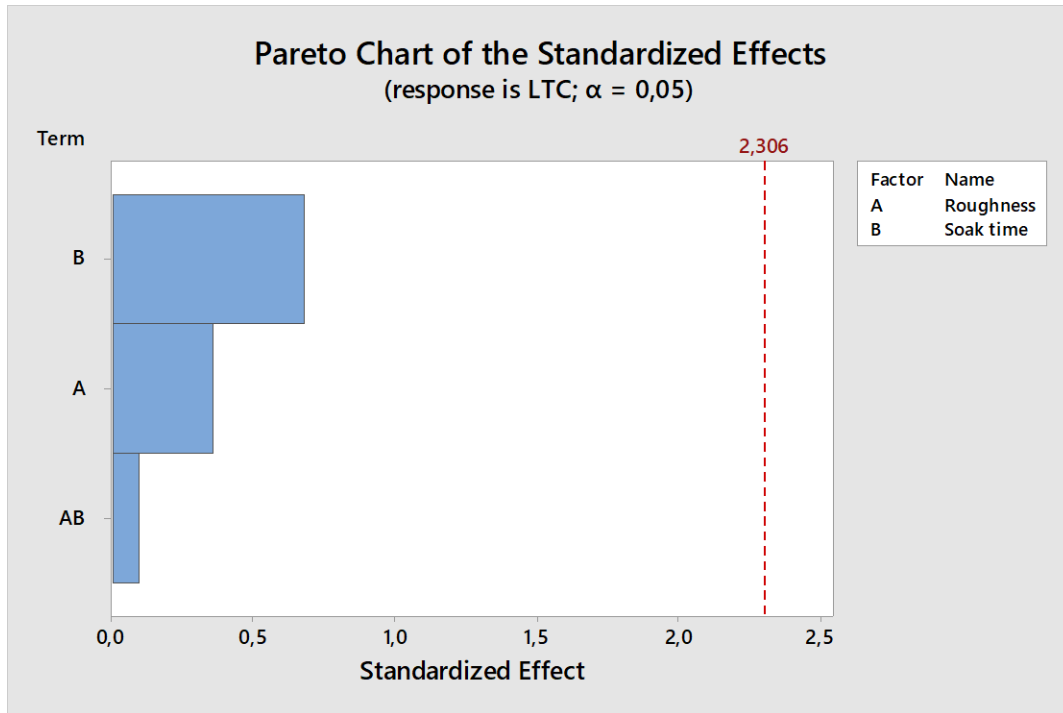


Figure 26 Pareto Chart for LTC of Al-Mg SLJ

Figure 25 and Figure 26 show how the SLJ LTC is influenced by the factors: the dotted red line represents the average LTC value of Al-Al and Al-Mg joints. Soak time is the most effective factor both for similar adherends SLJs and dissimilar adherends SLJs.

Figure 27 and Figure 28 represent how the surface roughness and soak time affect the LTC of the joints.

Table 8 summarizes and compares the results coming from the static tensile tests.

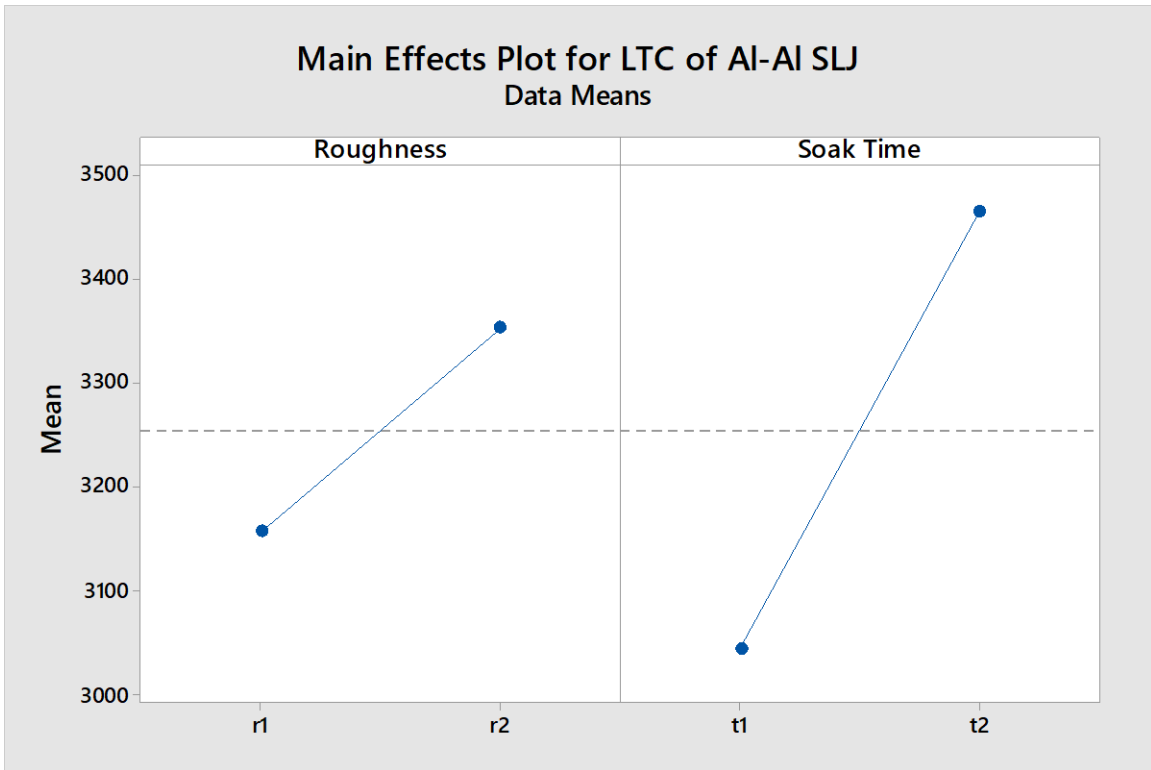


Figure 27 Main effects plot for LTC of Al-Al SLJ

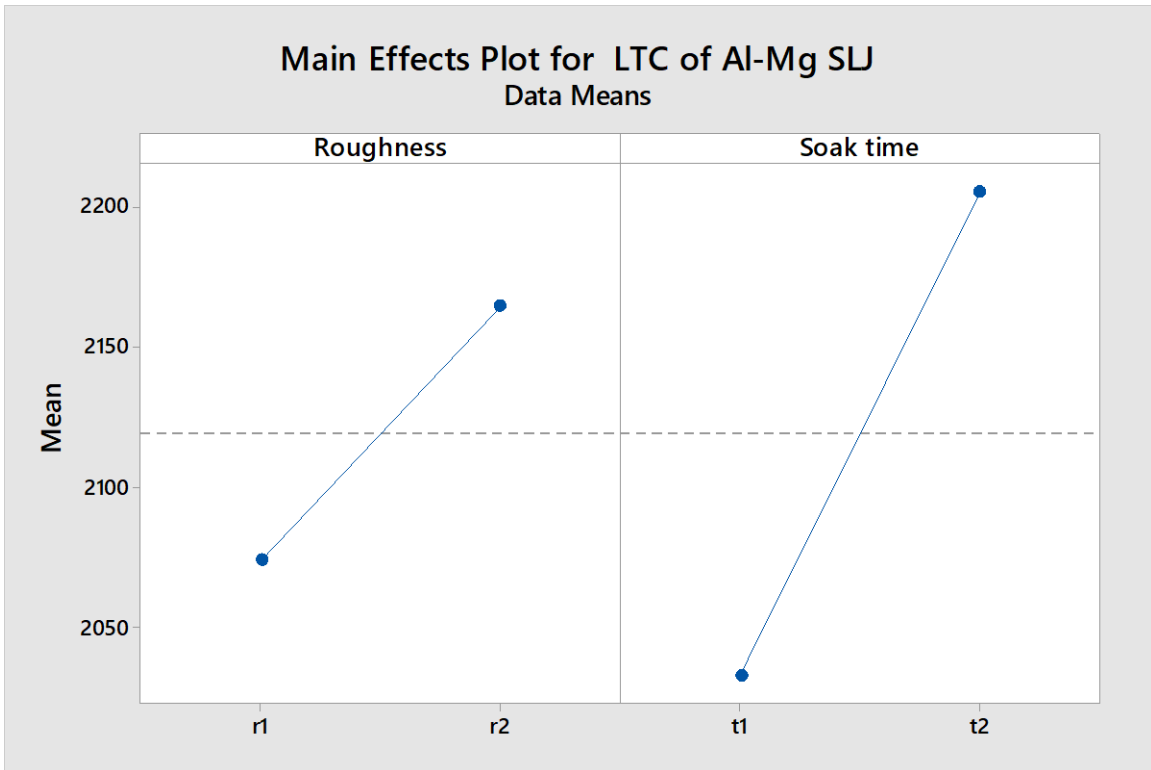


Figure 28 Main effects plot for LTC of Al-Mg SLJ

Table 8 LTC data comparison

Al Al t1							
roughness	average LTC [N]	stdev	% decrease in scatter from R1 to R2	% of LTC	% increase from R1 to R2	% increase from t1 to t2	% increase Al-Mg to Al-Al
R1	3045.0	421.9	-81.6	13.9	-0.1		52.2
R2	3042.0	232.4		7.6			47.2
Al Al t2							
R1	3266.8	369.0	-51.2	11.3	12.1	7%	52.1
R2	3661.4	244.0		6.7		20%	61.8
Al Mg t1							
R1	2000.3	248.1	2.3	12.4	3.3		
R2	2066.0	254.0		12.3			
Al Mg t2							
R1	2147.9	706.6	-82.9	32.9	5.3	7%	
R2	2262.7	386.2		17.1		10%	

The average LTC of the aluminum-aluminum SLJ is higher than the ones made of dissimilar adherends: the difference for all the combinations of roughness and cure time is around 50%, with almost 62% of increase for the case of higher roughness (R2) and higher soak time (t2).

A higher roughness level provides a higher LTC in comparison to lower roughness level, as it is shown in Table 8, except for the case of the similar adherends cured at the low soak time: in this case the average LTC is very similar and roughness seems not to affect its value.

Higher soak time provides a higher LTC in comparison to lower soak time: an increase of about 7% is shown for both combinations of material with lower roughness, 10% in case of dissimilar adherends with higher roughness, up to 20% in case of similar aluminum adherends and higher roughness.

By observing the Pareto charts we can notice that the roughness and the soak time effects are much less influential than the material of the adherends. The first Pareto graphs takes into account all the three factors analyzed while the other ones consider only roughness and soak time. The

author preferred to separate the results coming from aluminum-aluminum and aluminum-magnesium SLJ, since the material factor seems to overshadow all the others.

An important aspect that comes from the main effect plots is related to the roughness: the higher the roughness, the stronger the bond between adhesive and adherend and the higher the LTC. This fact can be explained through the mechanical interlock theory: the bond strength at the interface between the adherend and the adhesive is enhanced by the penetration of the polymer into the cavities and the pores of the substrate. The rougher the surface is, the higher the energy dissipation required for crack propagation is said to be, as it is stated by Kim et al. [10].

Failure mode and SEM inspection

After the execution of the shear-tensile tests and the evaluation of the LTC of the SLJs, the broken specimens were observed in order to understand which failure mode occurred.

By only observing the adherends surface, it is possible to say that all the SLJs were subjected to interfacial failure. In particular, for the case of dissimilar adherends, the adhesive always remains attached to the aluminum adherend and the interfacial failure occurs between magnesium adherend and polyurethane adhesive. This means that the strength of the bond is higher for aluminum alloy if compared to the magnesium alloy. Magnesium alloy has a worse affinity with the adhesive PE399 compared to aluminum alloy. As an example, Figure 29 shows the failure mode of the SLJs after they have been tested in shear-tensile static load.



Figure 29 Interfacial failure in Al-Mg SLJs

After the visual observation of the broken specimens, a Scanning Electron Microscope analysis has been performed on the adherends surface. An image of the INCA Scanning Electron Microscope is shown in figure 30.

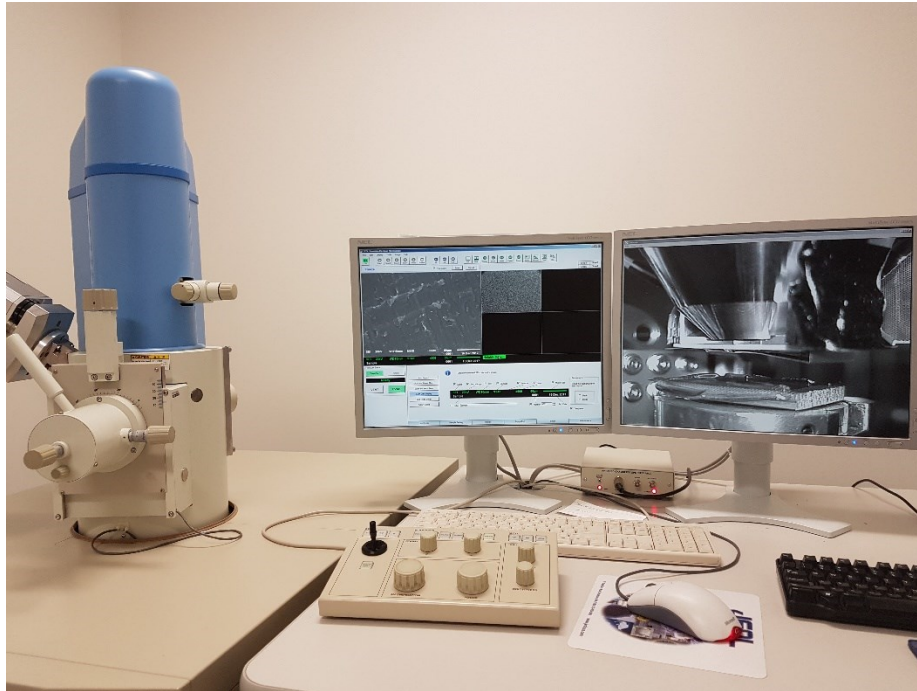


Figure 30 INCA Scanning Electron Microscope

The following pictures compare the surface of two joints taken as example: figure 31 represents the microscopic inspection of the aluminum adherend of an aluminum/aluminum SLJ, while figure 32 is the equivalent for the aluminum/magnesium SLJ.

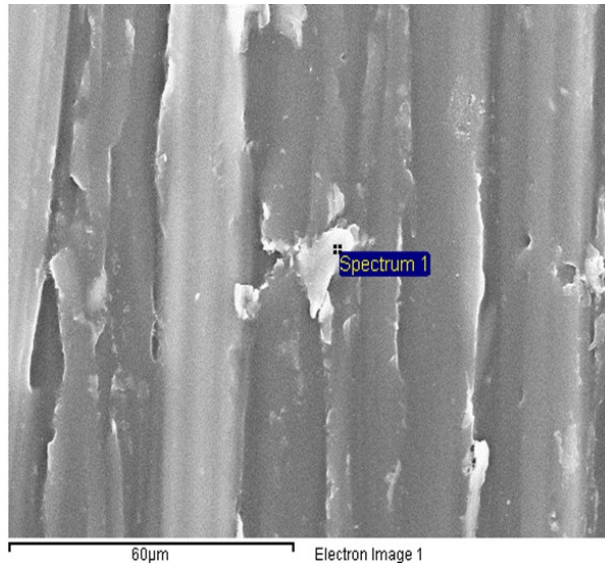


Figure 31 SEM analysis of Al-Al R2 ΔT1 SLJ (1000x)

From the picture above, it is evident the presence of straight lines due to the sand paper grinding of the adherend's surface. The lighter areas correspond to the presence of a high percentage of aluminum on the adhesive surface. This is due to metal transfer from the second adherend to the adhesive layer.

The spectral analysis gives a detailed information about the elements present on the adhesive surface in correspondence to the white spot in figure 31.

Table 9 Spectrum 1 of figure 31

Element	Weight%	Atomic%
O K	0.00	0.00
Al K	90.56	98.59
Au M	9.44	1.41
Totals	100.00	

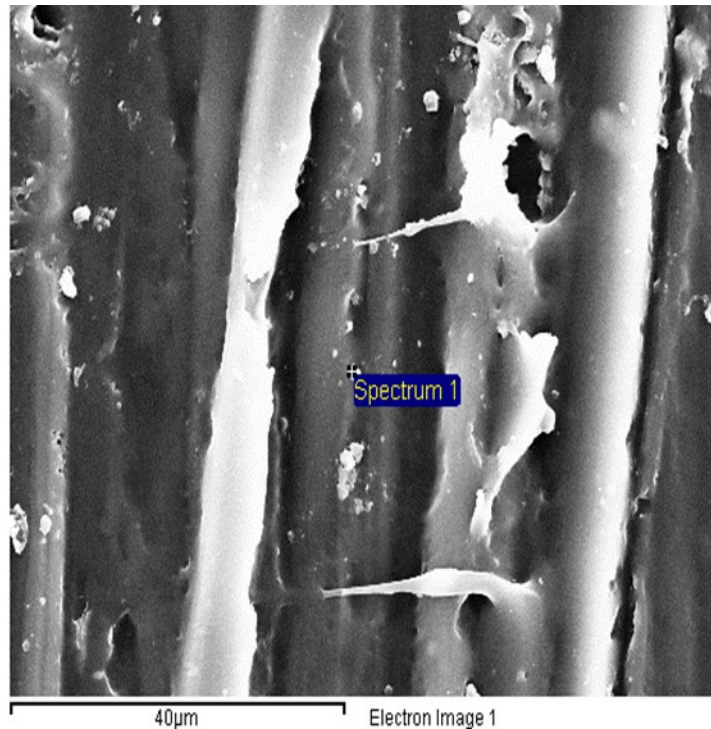


Figure 32 SEM analysis of Al-Mg R2 ΔT1 SLJ (250x)

Also in this case, the straight lines due to the sand-paper grinding are visible. It is worth noting that the horizontal white lines in Figure 32 demonstrate how the adhesive is pulled in the perpendicular direction, with respect to the tensile load.

The spectral inspection proves, also in this case, metal transfer (magnesium presence); the presence of carbon and oxygen are, with all certainty, due to the adhesive.

Table 10 Spectrum 1 of figure 32

Element	Weight %	Atomic %
C K	53.92	64.69
O K	35.23	31.73
Mg K	5.37	3.18
Al K	0.00	0.00
Au M	5.48	0.40
Totals	100.00	

Chapter 5

Cyclic tensile-shear testing and data analysis

The second part of the work consists of analyzing the effect of the same factors, namely roughness, soak time and material, on the fatigue strength in shear by tension loading of the SLJs. Durability tests have been carried out 24 hours after the autoclave cycle, all in the same day for each sample, when possible. Sometimes, in fact, one single test was lasting even four hours so it was impossible to test all the set of samples within the same day. The autoclave cycle parameters of the baking process to fabricate the SLJs, such as pressure and temperature profiles, correspond to the ones used for the preparation of the samples for the static tests.

All the fatigue tests have been carried out at a frequency of 20 Hz on the MTS machine. Usually low frequencies, in the range between 5 to 20 Hz, are recommended for adhesives. Higher frequencies could in fact affect and modify the viscoelastic properties of the adhesive and, consequently, alter the results.

Durability tests setup

Some screening tests were necessary in order to select the most appropriate fatigue cycle for the purpose of this work. The objective is to evaluate which factors affect the life of the joints most and what the intensity of their effect is.

In the first phase of durability tests, all the SLJs were tested under a sinusoidal fatigue cycle of the type represented in Figure 33: all the cycles ran at a mean force that corresponds to half of the SLJ LTC (α), while the amplitude corresponds to 2% of the LTC (β). The cycles were differentiated according to the LTC values obtained in the previous static tests as follows in Table 11.

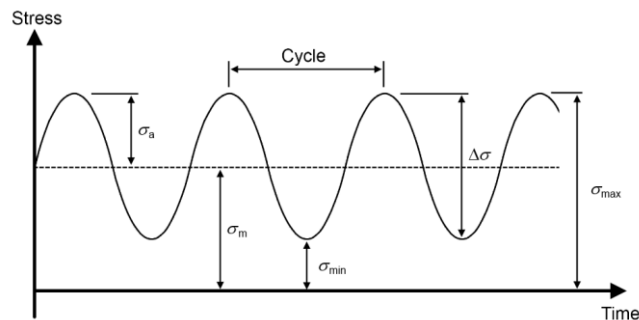


Figure 33 Cyclic load vs time

Table 11 Fatigue cycle parameters at low amplitude

SLJ parameters				Fatigue cycle low amplitude parameters			
Material	Soak Time	Roughness	Static LTC	α [% of LTC]	F mean [N]	β [% of LTC]	F alt [N]
Al-Al	Δt_1	R1	3045	50	1522	2	61
Al-Al	Δt_1	R2	3042	50	1521	2	61
Al-Al	Δt_2	R1	3267	50	1633	2	65
Al-Al	Δt_2	R2	3661	50	1831	2	73
Al-Mg	Δt_1	R1	2000	50	1000	2	40
Al-Mg	Δt_1	R2	2066	50	1033	2	41
Al-Mg	Δt_2	R1	2148	50	1074	2	43
Al-Mg	Δt_2	R2	2263	50	1131	2	45

As we can see from the table above, the fatigue tests have been carried out separately for similar and dissimilar adherends SLJs. The author decided to differentiate the cycles: from static analysis, in fact, the magnesium alloy has shown a weaker bond with the adhesive and, consequently, dissimilar joints have a lower LTC than the aluminum-aluminum SLJs.

It was meaningless to submit all the joints to the same fatigue cycle, because obviously the material would have affected the behavior and the fatigue life of the joints.

In the second phase of durability tests, in order to follow the purpose of looking at the effect of such factors on the fatigue life of the joints, only one cycle was chosen: all the aluminum-aluminum SLJs were submitted to the same cycle, and the same happened for the aluminum-magnesium SLJs. The mean force corresponds to half of the average value of the aluminum-aluminum SLJs LTC. The amplitude is 20 percent of their LTC, as well.

The same path has been followed for the dissimilar adherends SLJs, as it is summarized in Table 12: the mean force of the durability cycle corresponds to half of the average of aluminum-magnesium SLJs LTC and the amplitude is 20 percent of it.

Table 12 Fatigue cycle parameters at high amplitude

SLJ parameters				Fatigue load parameters			
Material	Cure Time [min]	Roughness [μm]	Static LTC [N]	α [% of LTC]	F_{mean} [N]	β [% of LTC]	F_{alt} [N]
Al-Al	40 and 80	R1 and R2	3254	50	1627	20	651
Al-Mg	40 and 80	R1 and R2	2119	50	1060	20	424

Test results of durability tests at low amplitude

The author decided to separate the results obtained from the Aluminum-Aluminum joints from the ones of aluminum-magnesium joints.

Tables 13 and 14 summarize the durability life of each specimen that was tested under the cyclic load at an amplitude of 2% of the SLJs LTC. The same results with their relative scatter are presented in the graphs of Figure 34 and Figure 35.

Table 13 Durability life of Al-Al SLJ tested at low amplitude

SLJ type	specimen	cycles to failure
Al-Al t1 R1	a	23726
	b	80096
	c	69205
Al-Al t1 R2	a	18636
	b	52261
	c	7598
Al-Al t2 R1	a	86756
	b	30894
	c	179945
Al-Al t2 R2	a	33974
	b	6978
	c	49166

Table 14 Durability life of Al-Mg SLJ tested at low amplitude

SLJ type	specimen	cycles to failure
Al-Mg t1 R1	a	5293
	b	89710
	c	169868
Al-Mg t1 R2	a	87880
	b	50635
	c	31598
Al-Mg t2 R1	a	15365
	b	112588
	c	485277
Al-Mg t2 R2	a	123713
	b	101396
	c	110140

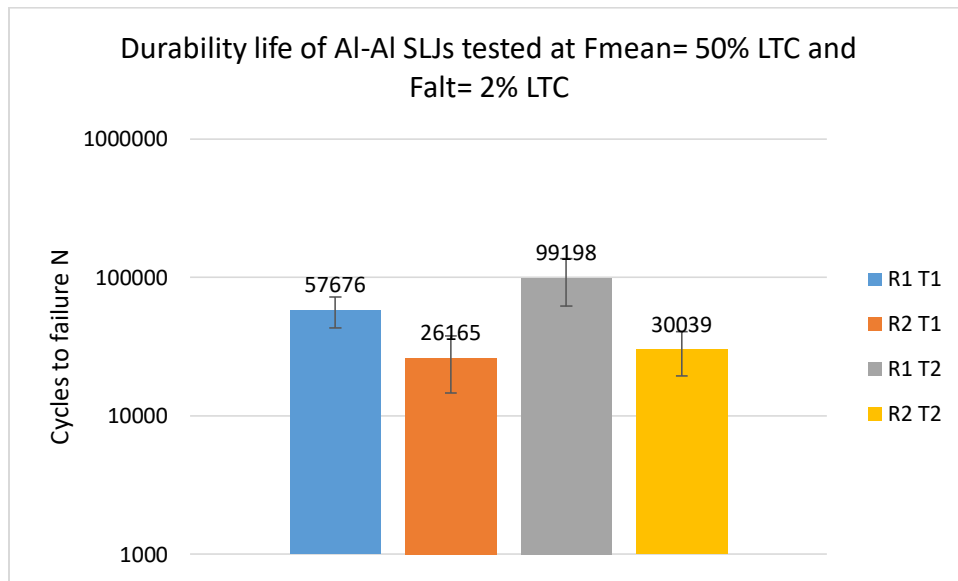


Figure 34 Durability life of Al-Al SLJ tested at low amplitude

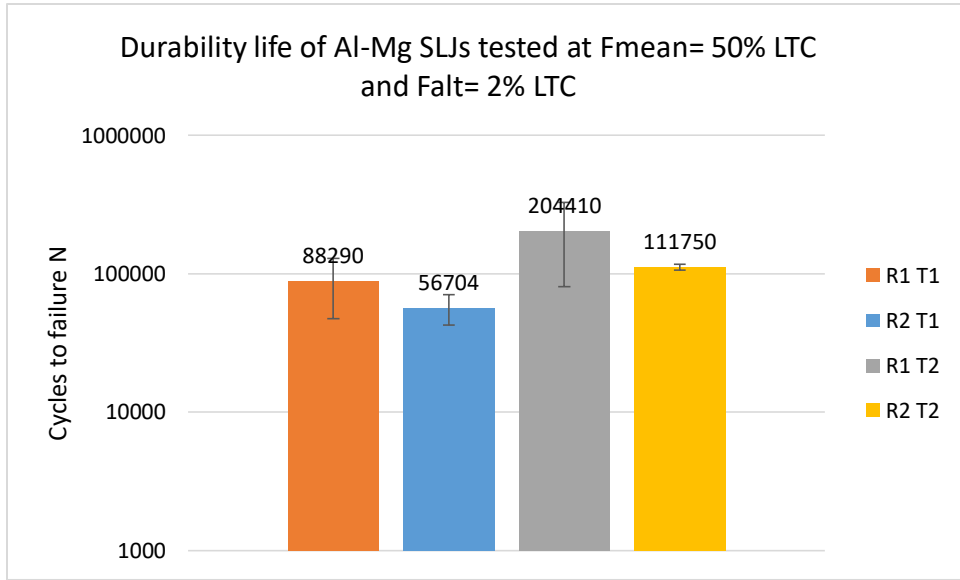


Figure 35 Durability life of Al-Mg SLJ tested at low amplitude

Statistical analysis of the durability life of SLJs tested at low amplitude

This section provides a statistical analysis of the results obtained from the fatigue tests of SLJs.

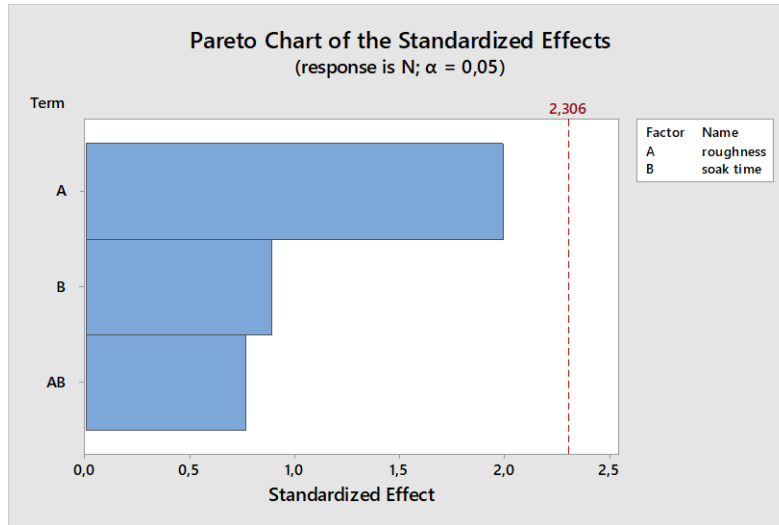


Figure 36 Pareto Chart for durability life of Al-Al SLJ tested at low amplitude

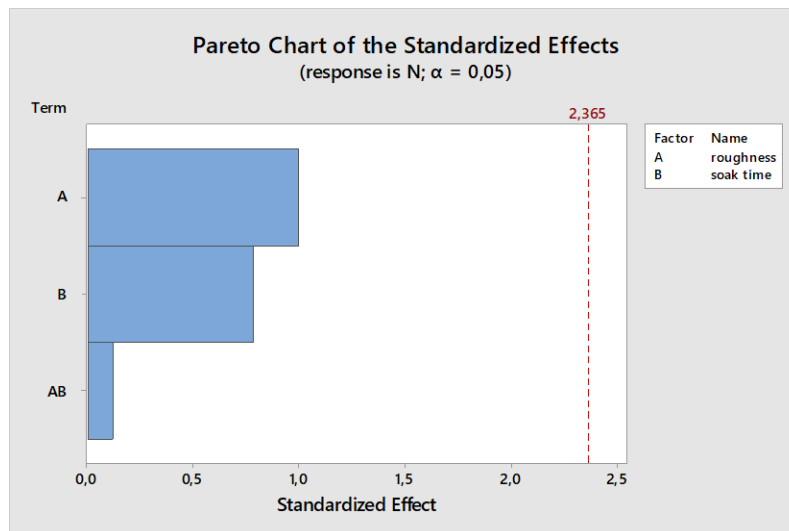


Figure 37 Pareto Chart for durability life of Al-Mg SLJ tested at low amplitude

By observing the data and the graphs above, it is clear that both of the factors analyzed are below the noise level. This means that their influence on the durability life of the joints is not relevant.

It is important to notice that both for aluminum-aluminum and aluminum-magnesium SLJs the roughness is more relevant than the soak time. In addition, it is worth to notice that the roughness affects the fatigue performance of the joints in an opposite way with respect to what happened during the static tests.

By looking at the main effects plots in Figure 38 and Figure 39, in facts, a smoother surface (R1) provides longer durability life both for the case of similar and dissimilar SLJs.

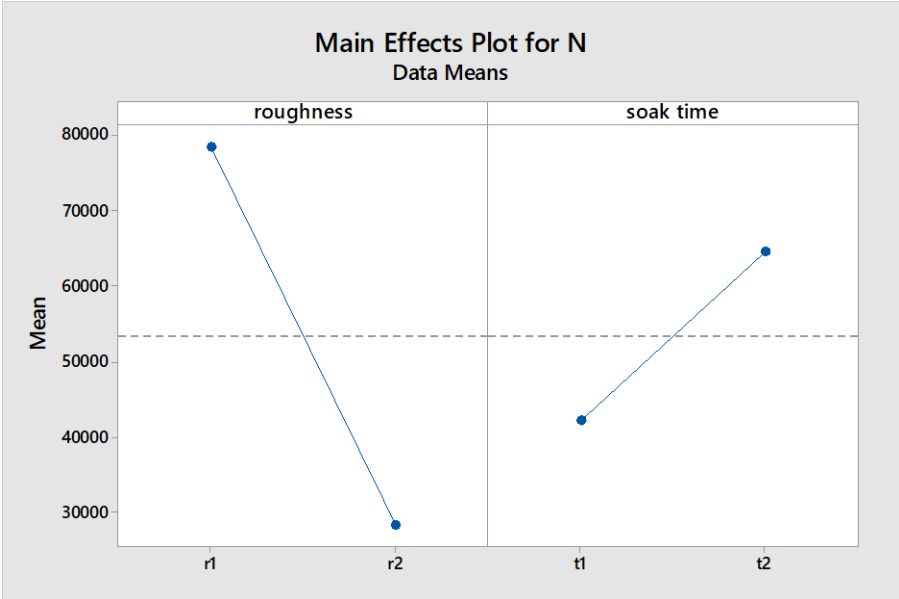


Figure 38 Main effects plot for durability life of Al-Al SLJ tested at low amplitude

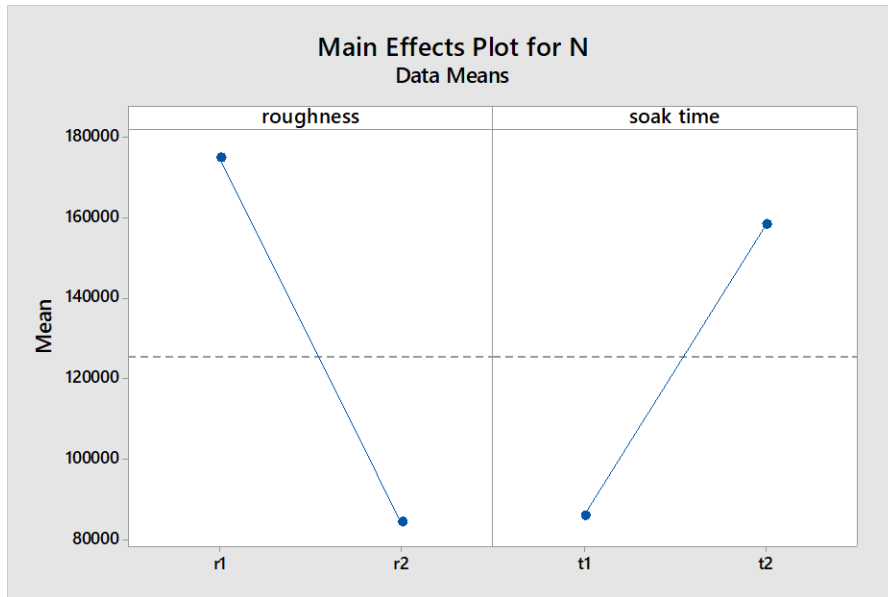


Figure 39 Main effects plot for durability life of Al-Mg SLJ tested at low amplitude

Test results of durability tests at high amplitude

Also for the case of high amplitude, the author decided to separate the results obtained from the Aluminum-Aluminum joints from the ones of aluminum-magnesium joints. This set of tests differs from the previous one because the fatigue cycles do not differ according to soak time and roughness levels: this means that one single cycle has been performed on all the similar-adherends joints, and one single cycle has been performed on all the dissimilar-adherends joints.

The average force (F_{mean}) corresponds to half of the average static LTC of the joints, and the amplitude corresponds to a fixed percentage of it.

Table 15 and Table 16 show the cycles to failure of similar and dissimilar adherends SLJ tested under high amplitude load condition; Figure 40 and Figure 41 represent the average of the same results, with their relative scatter.

Table 15 Durability life of Al-Al SLJ tested at high amplitude

SLJ type	specimen	cycles to failure
Al-Al t1 R1	a	8367
	b	6140
	c	9466
Al-Al t1 R2	a	2699
	b	5006
	c	967
Al-Al t2 R1	a	23004
	b	135069
	c	12045
Al-Al t2 R2	a	3790
	b	13763
	c	101760

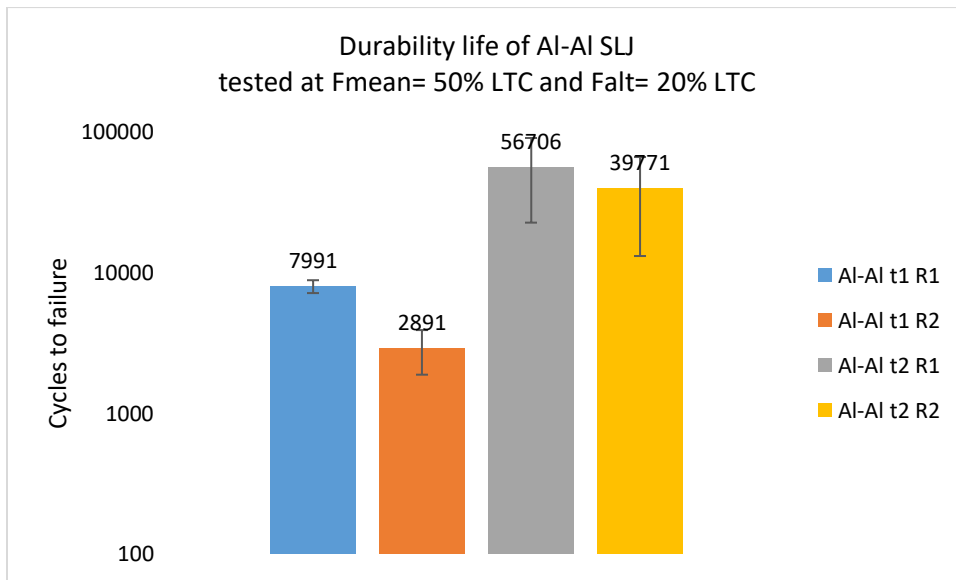


Figure 40 Durability life of Al-Al SLJ tested at high amplitude

Table 16 Durability life of Al-Mg SLJ tested at high amplitude

SLJ type	specimen	cycles to failure
Al-Mg t1 R1	a	23307,00
	b	17392,00
	c	18604,00
Al-Mg t1 R2	a	11020,00
	b	11718,00
	c	6896,00
Al-Mg t2 R1	a	57882,00
	b	125249,00
	c	39903,00
Al-Mg t2 R2	a	11917,00
	b	16753,00
	c	66101,00

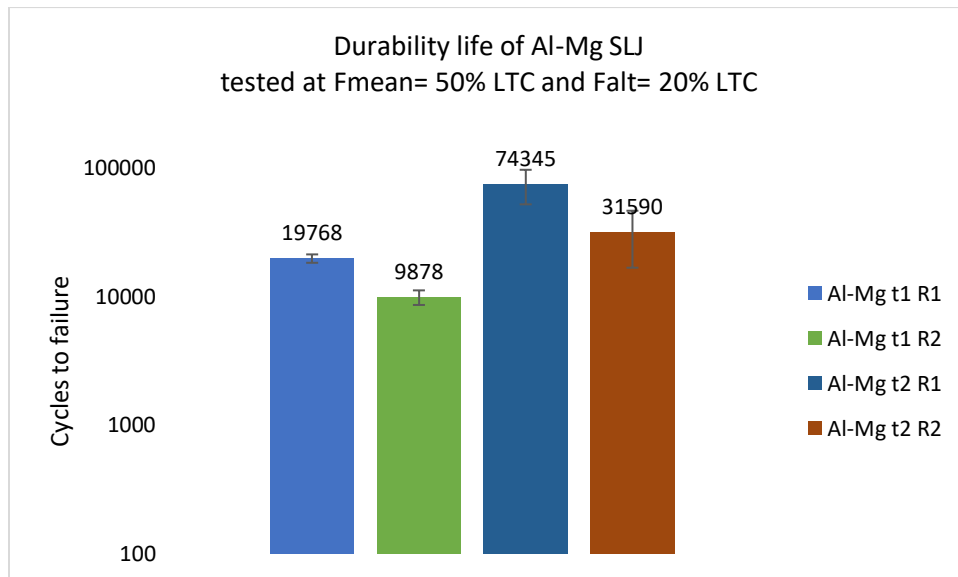


Figure 41 Durability life of Al-Mg SLJ tested at high amplitude

Statistical analysis of the durability life of SLJs tested at high amplitude

As for the case of low amplitude durability cycles, a statistical analysis has been run and the Pareto charts in Figure 42 and Figure 44 show the most significant effect among the surface roughness and the soak time. Both for the case of aluminum-aluminum SLJ and aluminum-magnesium SLJ the soak time is the most important factor; it is above the noise level in case of dissimilar adherends and, for both the cases, it affects the durability life in terms of cycles to failure (N) in the same way as it affected the joints LTC.

Figure 43 and Figure 45 show how a longer soak time during the autoclave process reinforces the adhesive bond and ensures a longer life in term of cycles to failure.

The above cited figures also show the inversion of trend related to the surface roughness effect on the durability life: also in the case of high amplitude cyclic load, the smoother surface provides a better performance in terms of cycles to failure.

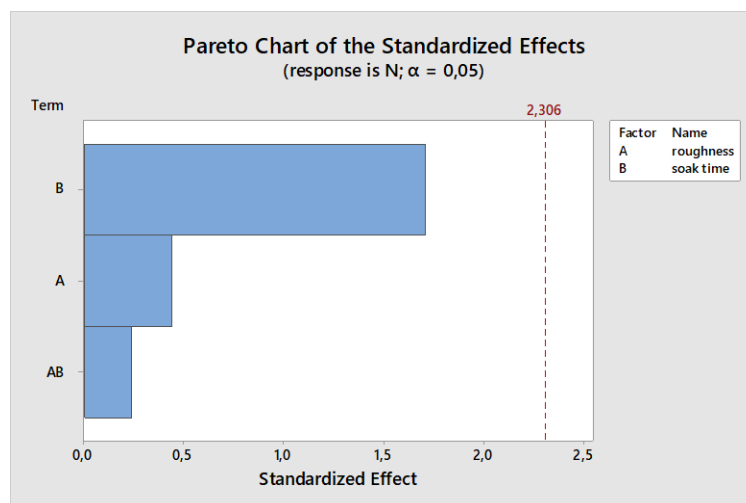


Figure 42 Pareto Chart for durability life of Al-Al SLJ tested at high amplitude

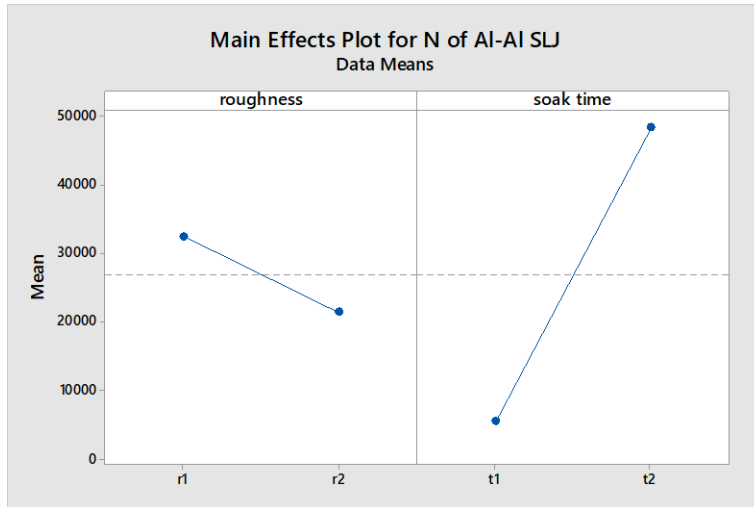


Figure 43 Main effects plot for durability life of Al-Al SLJ tested at high amplitude

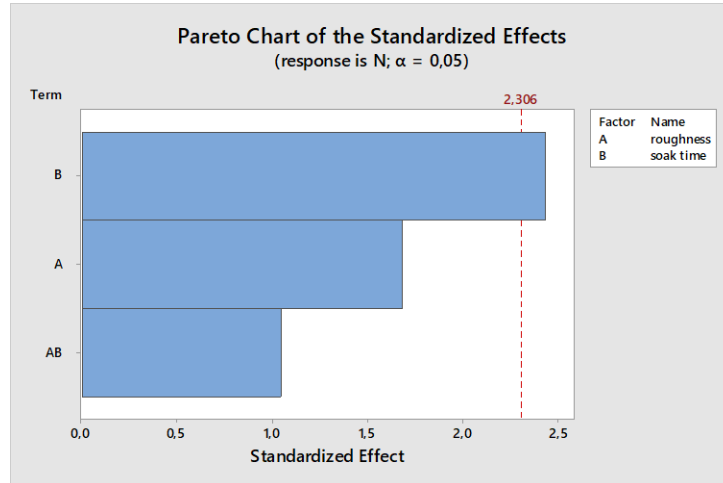


Figure 44 Pareto Chart for durability life of Al-Mg SLJ tested at high amplitude

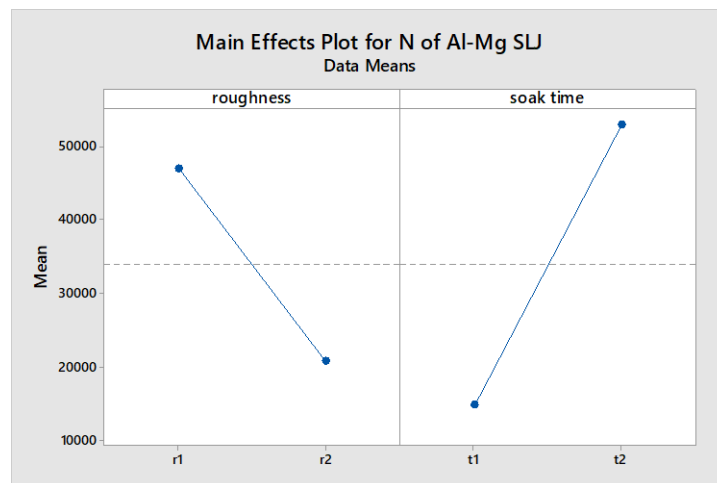


Figure 45 Main effects plot for durability life of Al-Mg SLJ tested at high amplitude

Figure 46 and Figure 47 show the totality of results coming from the durability tests made at an amplitude of 20% of the joints LTC.

Some observation and conclusions are provided:

- Material is the least effective between all the three factors because the parameters of the fatigue cycles (F_{mean} and F_{ait}) are normalized according to it.
- Soak time is the most important effect and the behavior of the joints confirms the trend obtained through the static tests to evaluate the LTC of the joints.
- Surface roughness gives an inverse trend with respect to static data: a rougher surface does not guarantee a stronger adhesive bond. A possible explanation of this phenomenon is that the asperities of the surface operate as cracks initiator and they promote the failure of the adhesion at the interface.

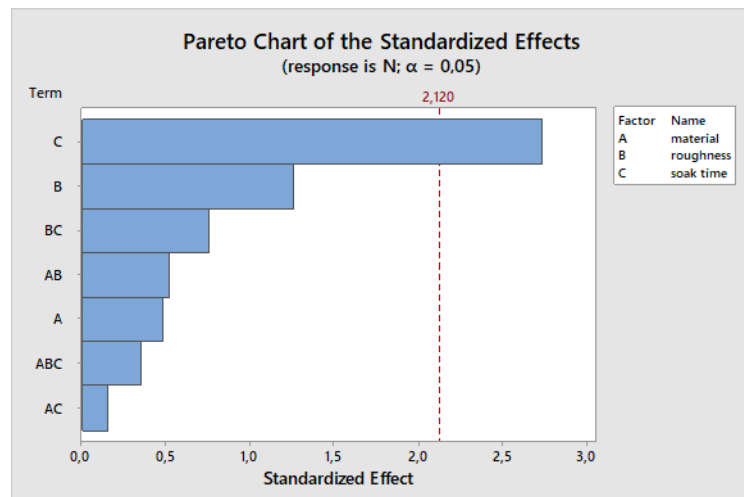


Figure 46 Pareto Chart for durability life of Al-Al and Al-Mg SLJ tested at high amplitude

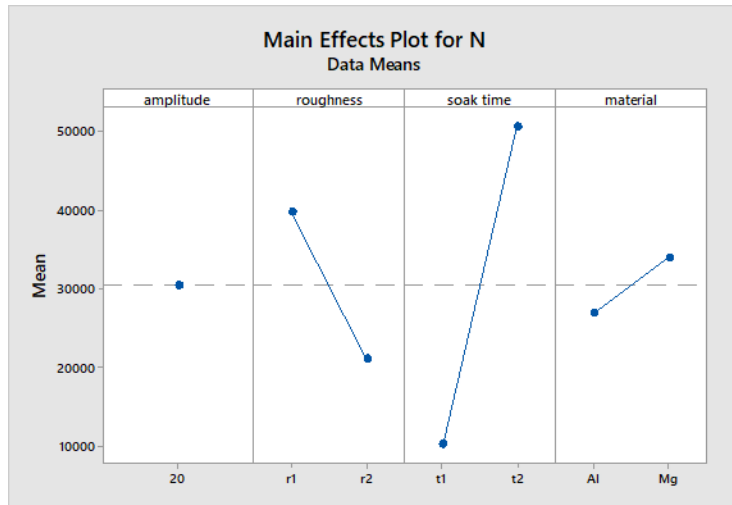


Figure 47 Main effects plot for durability life of Al-Al and Al-Mg SLJ tested at high amplitude

S-N curves

In this chapter the S-N curves of the SLJs tested under cyclic tensile-shear load are presented. In the same graph, data coming from aluminum-aluminum and aluminum-magnesium SLJs are shown, in order to make a comparison and to observe the difference in fatigue life between similar and dissimilar joints. It is worth to underline that the joints were tested at the same relative percentage of force, according to the respective LTC.

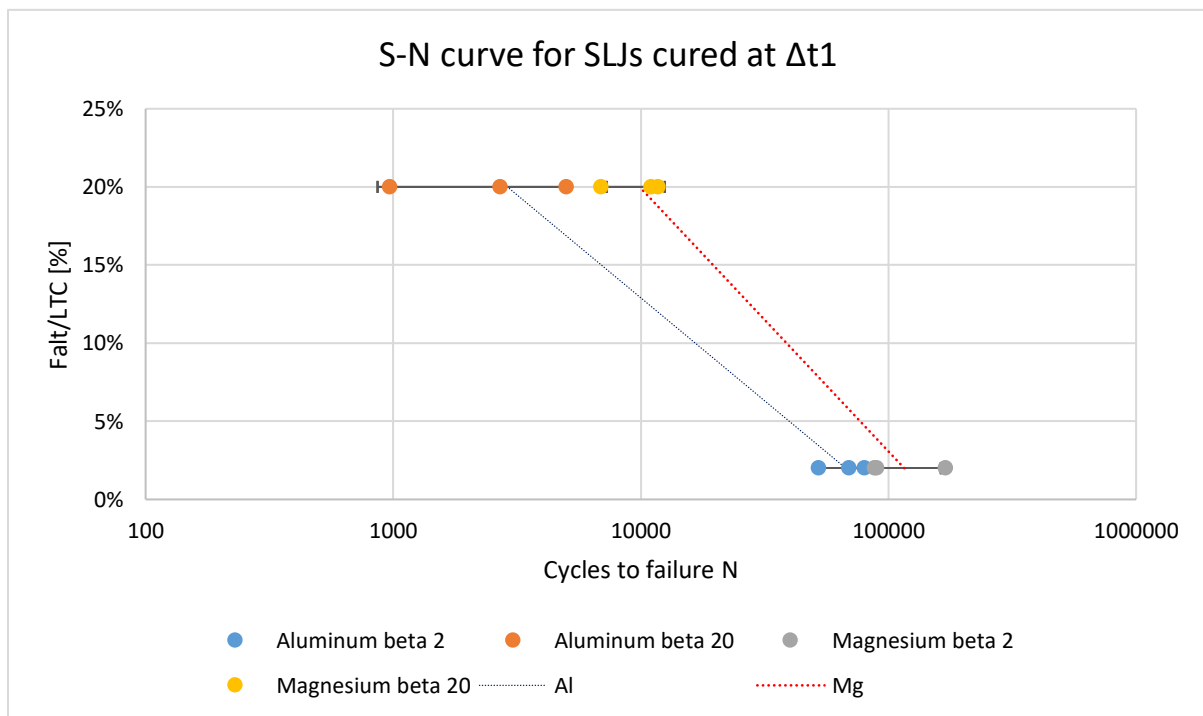


Figure 48 S-N curve of SLJs cured at ΔT_1

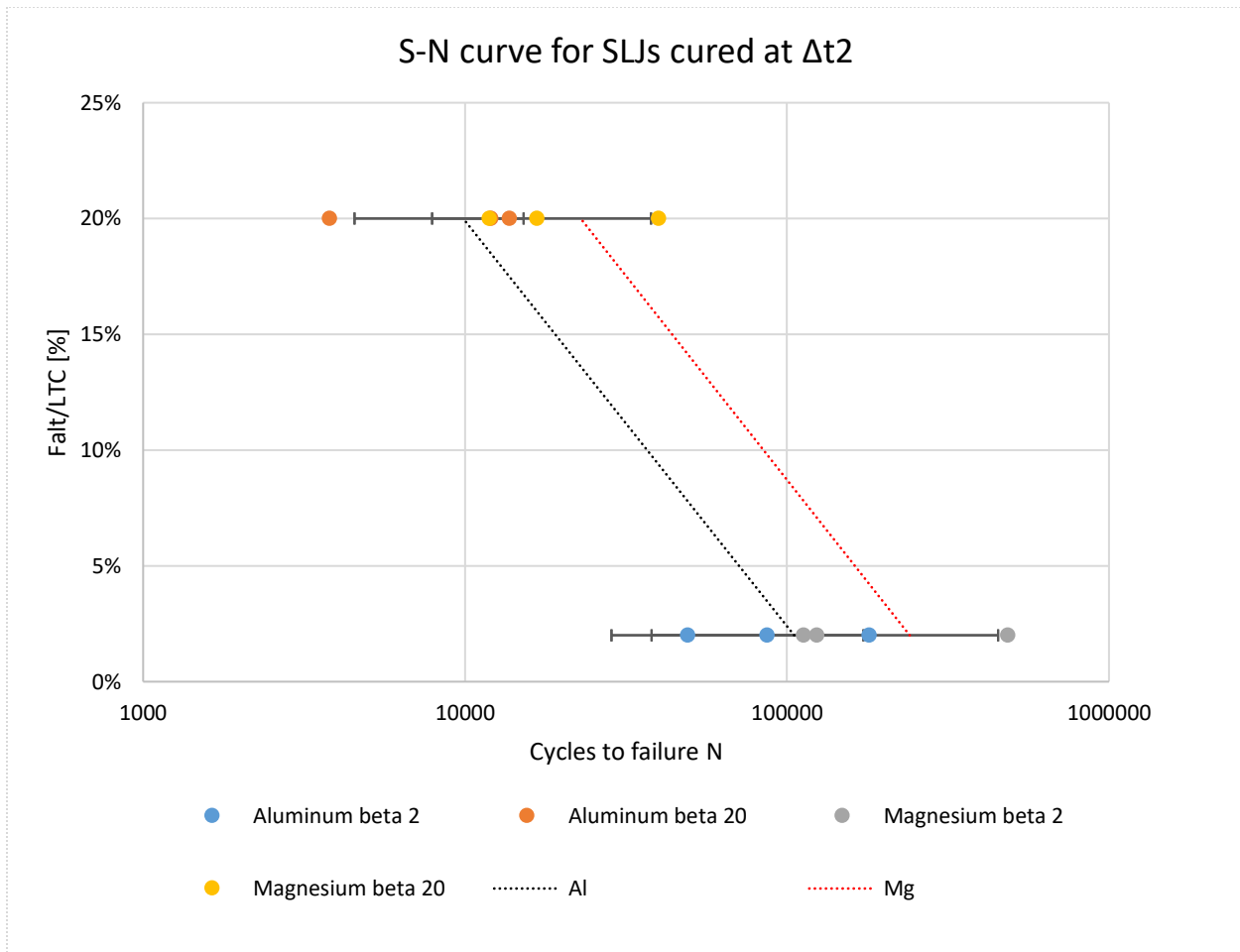


Figure 49 S-N curve of SLJs cured at ΔT_2

Figure 48 and Figure 49 show the fatigue life in terms of cycles to failure (N) of different joints tested at a mean force $F_{\text{mean}} = 50\%$ LTC, with a variable force F_{alt} equal to 2% or 20% of their relative LTC. In fact, all the fatigue cycles were normalized according to the static LTC of the joints.

The label “beta 2” or “beta 20” refer to the amplitude of the force F_{alt} in the cyclic load: 2% or 20% of the normalized LTC.

Even if the life of dissimilar adherends joints is clearly higher than similar ones’ life, the difference in terms of cycles to failure (N) still falls within the range of statistical scatter for fatigue life.

Failure mode and SEM inspection

After the execution of the shear-tensile tests under cyclic load, the broken specimens were observed in order to understand which failure mode occurred. By only looking at the adherends surface, it is observed that all the SLJs broke with interfacial failure also in this case.

As an example, in the following paragraph the analysis conducted on two different SLJs will be presented: the first one refers to the aluminum/aluminum SLJ tested under cyclic load, while the second refers to the aluminum/magnesium SLJ tested under the same conditions. Obviously, to compare properly the two samples, two joints with the same characteristics in terms of surface roughness and cure time have been chosen.

Aluminum-aluminum SLJ

The following image in Figure 50 is an enlargement of one of the adherends of the aluminum/aluminum SLJ tested in fatigue. The adhesive surface was analyzed through the electron microscope and the spectrum 1 in the figure above proves that metal transfer happened.

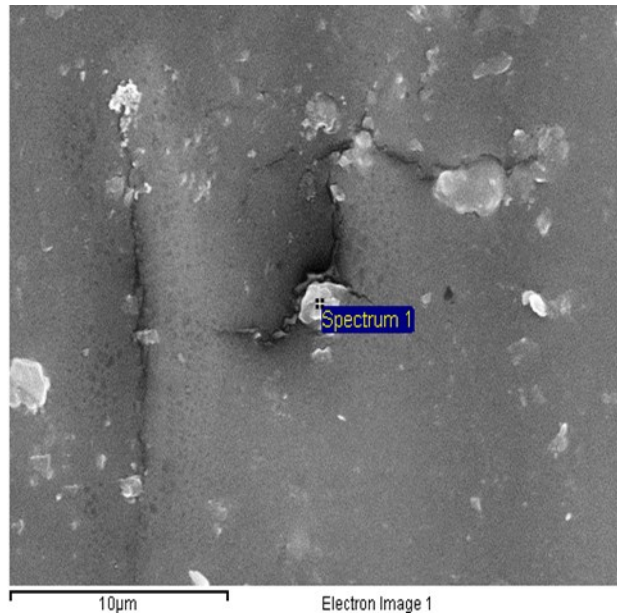


Figure 50 SEM analysis of Al-Al SLJ R1 (1000x) adhesive side

It is worth to notice the presence of a crack on the adherend surface; this is the cause of the adhesion failure at the aluminum-polyurethane interface. The aluminum metal particles that come from the degradation of the second aluminum adherend are the white areas on the adhesive surface in figure 50.

The spectrum of Table 17 that refers to the bright spot in figure 50 pointed out presence of aluminum, gold and oxygen.

Table 17 Spectrum 1 of figure 50

Element	Weight%	Atomic%
C K	0.00	0.00
O K	48.14	66.05
Mg K	0.00	0.00
Al K	40.12	32.64
Au M	11.75	1.31
Totals	100.00	

Aluminum-magnesium SLJ

Figure 51 examines the adhesive surface on the aluminum side of the dissimilar adherend joint.

The SEM analysis at low magnification (200x) did not detect the presence of other elements than oxygen and gold, which comes from the high energy beam of electrons sent to the sample.

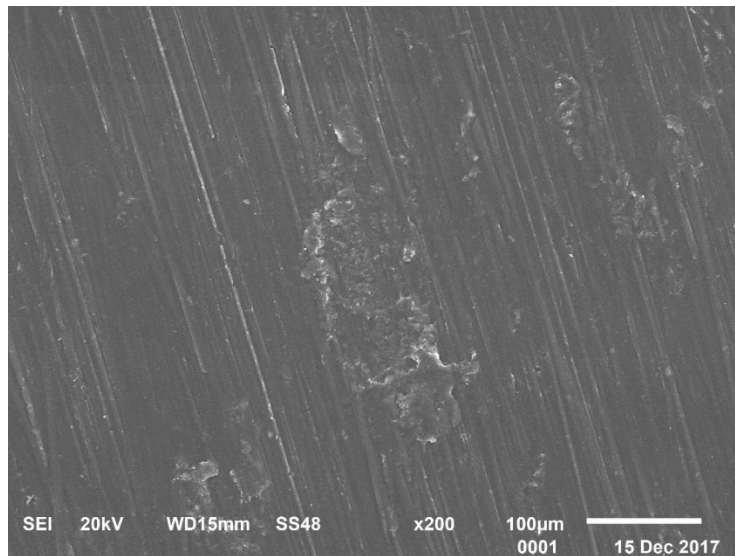


Figure 51 SEM analysis of Al-Mg SLJ R1 (200x) Al side

A higher magnification (3000x) detected the presence of magnesium on the same sample, as shown in Figure 52.

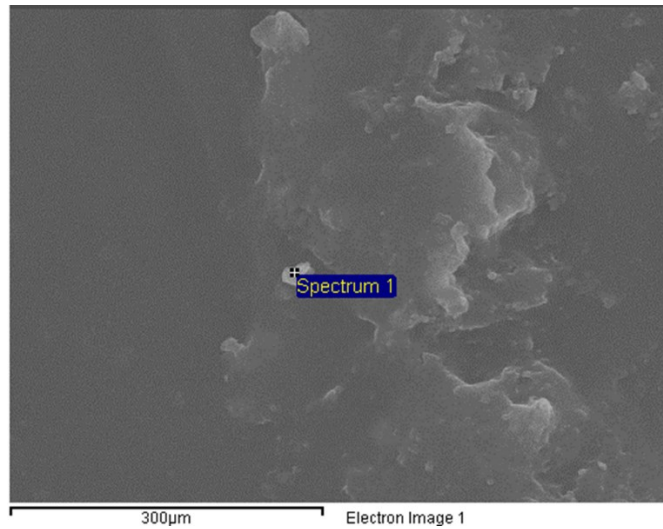


Figure 52 SEM analysis of Al-Mg SLJ R1 (3000x) Al side

Table 18 Spectrum 1 of figure 52

Element	Weight%	Atomic%
C K	0.00	0.00
O K	66.85	81.23
Mg K	22.11	17.68
Al K	0.00	0.00
Au M	11.05	1.09
Totals	100.00	

The following pictures analyze two different spots of the same sample as before. The lighter area that is analyzed in spectrum 1 highlights magnesium presence, while the darker area in spectrum 2 does not show the presence of magnesium.

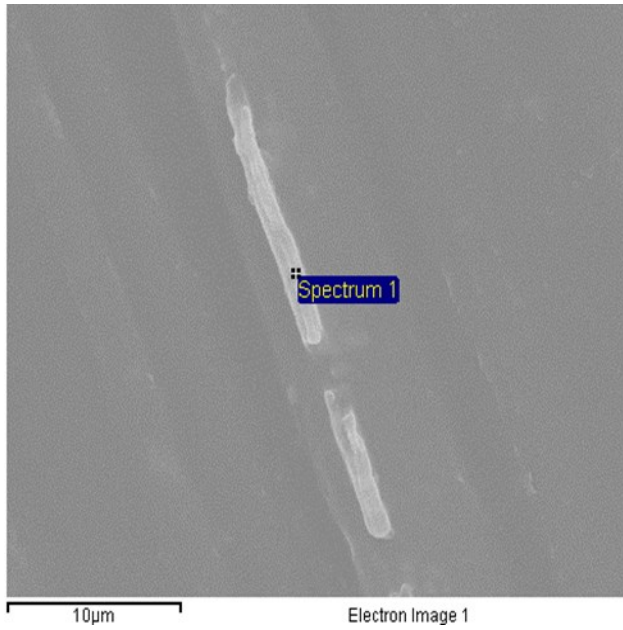


Figure 53 SEM analysis of Al-Mg SLJ R1 (1500x) Al side

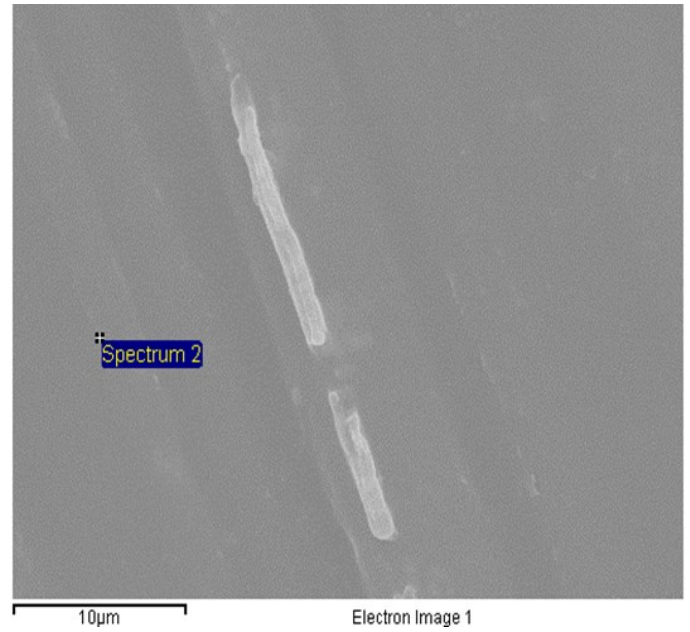


Figure 54 SEM analysis of Al-Mg SLJ R1 (1500x) Al side

Table 19 Spectrum 1 and spectrum 2 of figures 53 and 54

Spectrum 1			Spectrum 2		
Element	Weight%	Atomic%	Element	Weight%	Atomic%
C K	0.00	0.00	C K	0.00	0.00
O K	64.81	83.17	O K	74.13	97.24
Mg K	17.79	15.02	Mg K	0.00	0.00
Al K	0.00	0.00	Al K	0.00	0.00
Au M	17.40	1.81	Au M	25.87	2.76
Totals	100.00		Totals	100.00	

The comparison between the aluminum/aluminum joint adherend and the aluminum/magnesium allows to underline some differences:

- Magnesium particles are not widespread as the aluminum ones in the adherends
- Cracks are clearly evident only on the aluminum/aluminum joint adherend and this can be taken as explanation of the lower fatigue life in case of similar adherends joints

It is worth to observe also the magnesium surface of the same joint. It is clearly visible the presence of holes (darker areas), which confirm the metal transfer from one adherend to the other.

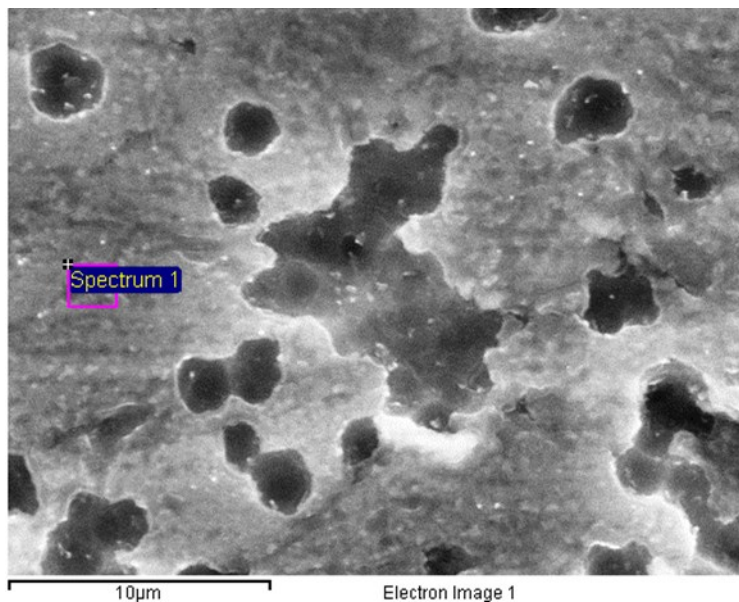


Figure 55 SEM analysis of Al-Mg SLJ R1 (250x) Mg side

Table 20 Spectrum 1 of figure 55

Element	Weight%	Atomic%
C K	0.00	0.00
O K	16.16	22.65
Mg K	83.84	77.35
Al K	0.00	0.00
Totals	100.00	

Also in the case of cyclic tensile-shear load, when the joint is made of dissimilar adherends, the adhesive always remains attached to the aluminum adherend and the interfacial failure occurs between magnesium adherend and polyurethane adhesive. This confirms that the strength of the bond is higher for aluminum alloy if compared to the magnesium alloy and that magnesium alloy has a worse affinity with the adhesive PE399 compared to aluminum alloy.

The SEM analysis on the SLJs tested in cyclic tensile-shear shows a higher percentage of transferred metal on the adhesive surface in case of aluminum-aluminum SLJ when compared to aluminum-magnesium SLJ. This explains the higher degradation of the bond between adhesive and adherend in case of aluminum-aluminum SLJ tested in cyclic load. The higher degradation of the bond of similar adherends joints tested under cyclic load compared to dissimilar adherends joints is taken as a possible explanation of the aluminum-magnesium coupons longer life, although the difference in their average number of cycles to failure still falls within the range of the statistical scatter for fatigue life under the same cyclic load condition (relatively to their own

LTC). Among the principal causes of metal transfer on the adhesive during cyclic loading there is the degradation of the metal oxide-layer due to the fretting at the interface.

Conclusion

This study provides an insight into the characterization of the mechanical behavior of adhesive SLJs made of lightweight metallic alloys, when they are tested in tensile-shear static and cyclic load. Beyond this purpose, the main objective of the work is the analysis of how and with what intensity the surface roughness at the adherend/adhesive interface and the curing time of the bonding procedure affect the performances of the joints.

It has been observed that longer cure time (80 minutes vs 40 minutes) during the autoclave bonding process increased the static LTC of test joints by an average of 13.5%. Higher surface roughness of the bond area led to a higher static LTC of test joints: the higher increase is observed in case of aluminum-aluminum joints cured at ΔT_2 , with a percentage increase of 12%. This is due to the stronger interlock between the larger adherend asperities and the film adhesive. The static LTC of similar aluminum-aluminum test joints is much higher than that of the dissimilar joints in aluminum-magnesium: whatever the cure time and/or surface roughness, the increase is always higher than 50%. This is caused by a stronger adhesion between aluminum adherend and adhesive than between magnesium adherend and adhesive.

All the test samples under static tensile load fractured with interfacial failure mode and it was observed that the interfacial failure in case of dissimilar SLJs always happened on the magnesium adherend's side.

Under a cyclic tensile-shear load with a mean load of 50% of static LTC, a longer cure time led to a higher fatigue life due to improved bonding strength.

However, a reversed behavior is observed when the roughness effect is taken into account: the increased surface roughness lowered the fatigue life. This can be explained by considering the asperities of the surface as crack initiators.

SEM analysis proved the presence of aluminum or magnesium on the adherend in aluminum or magnesium, respectively. This means that metal particles transfer from the adherend to the adhesive. The phenomenon was observed in the joints which came from static tensile test as well as from cyclic tests. The phenomenon can be more or less uniform and widespread; on the aluminum surface of the joints was observed a higher quantity of metal particles and this was taken as explanation of the lower fatigue life of similar joints.

On the surface of aluminum and magnesium joints the presence of oxygen was proved after the SEM analysis. This confirms the oxidation of both the alloys.

In case of dissimilar adherends, the magnesium side was observed too and it proved the existence of holes and porosities that are due to the surface oxide layer degradation at the interface.

Future work

The objectives of this work are the evaluation of the effects of some factors, namely the surface roughness of the adherends and the adhesive cure time, on the behavior of SLJs under static and cyclic tensile-shear stress. The importance of the characterization of the lightweight material adhesive joints in automotive makes necessary a deeper research in this field.

Future works could extend the same analysis to other lightweight materials used in the automotive field, such as titanium, carbon fiber composites, and advanced high strength steels (AHSS).

Aluminum 6061 alloy and magnesium AZ31B alloy have been chosen because of the local availability, and two combinations of them have been investigated: similar adherends (aluminum-aluminum) and dissimilar adherends (aluminum-magnesium). The option magnesium-magnesium SLJ has not been studied: it would be interesting to analyze the mechanical performances in this case.

In this study the surface roughness of the adherends has been achieved by hand through the use of sand-paper: smoother and more uniform levels of roughness (R_a) could be achieved by ultrasonic polishing, magnetic polishing or sandblasting. On the other side, a rougher surface can be obtained by using photolithography in order to have micro-lined patterned surfaces with a precise morphology, following the path that has been taken by Kim et al. [10]

References

- [1] A. Baldan, «Adhesion phenomena in bonded joints,» *International Journal of Adhesion & Adhesives*, pp. 95-116, 2012.
- [2] M. K. Kulekci, «Magnesium and its alloys applications in automotive industry,» *International Journal Advanced Manufactory Technology*, pp. 851-865, 2008.
- [3] Energy.gov, «Energy.gov,» 25 August 2016. [Online]. Available:
<https://energy.gov/eere/articles/timeline-path-lightweight-materials-cars-and-trucks>.
- [4] *Lecture notes of the course 'Controllo delle emissioni di inquinanti'*, Politecnico di Torino, 2016.
- [5] S. Wu, «Polar and Nonpolar Interactions in Adhesion,» *The Journal of Adhesion*, pp. 39-55, 2006.
- [6] Adhesive and Sealant Council, «Adhesives.org/Sealants.org,» 2008. [Online]. Available:
<http://www.adhesives.org/adhesives-sealants/science-of-adhesion/adhesion-cohesion>.
- [7] A. Baldan, «Review Adhesively-bonded joints and repairs in metallic alloys, polymers and composite materials: Adhesives, adhesion theories and surface pretreatment,» *Journal of Material Science*, pp. 1-49, 2004.
- [8] S. Ebnesaajad e A. H. Landrock, *Adhesives Technology Handbook*, Elsevier, 2009.
- [9] R. A. Flinn e P. K. Trojan, *Engineering Materials and their Application*, 1995.
- [10] Y. L. Y. Kim, «Evaluation of mechanical interlock effect on adhesion strength of polymer-metal interfaces using micro-patterned surface topography,» *International Journal of Adhesion and Adhesives*, vol. 30, pp. 408-417, 2010.

- [11] A. J. Kinloch, *Adhesion and Adhesives Science and Technology*, Springer, 1987.
- [12] Adhesive and Sealant Council, «Adhesives.org/Sealants.org,» 2008. [Online]. Available:
<http://www.adhesives.org/adhesives-sealants/science-of-adhesion/surface-treatment>.
- [13] R. Smerd, S. Winkler, C. Salisbury, M. Worswick, D. Lloyd e M. Finn, «High strain rate tensile testing of automotive aluminum,» *International Journal of Impact Engineering* 32, 2005.
- [14] A. Pereira, P. Reis, J. Ferreira e F. Antunes, «Effect of saline environment on mechanical properties of adhesive joints,» *International Journal of Adhesion & Adhesives* 47, pp. 99-104, 2013.
- [15] M. Banea e L. da Silva, «The effect of temperature on the mechanical properties of adhesives for the automotive industry,» *Proc. IMechE*, vol. 224, pp. 51-62, 2009.
- [16] E. Knox e M. Kowling, «Durability aspects of adhesively bonded thick adherend lap shear joints,» *International Journal of Adhesion & Adhesives* 20, pp. 323-331, 2000.
- [17] I. Pires, L. Quintino, J. F. Durodola e A. Beevers, «Performance of bi-adhesive bonded aluminium lap-joints,» *International Journal of Adhesion and Adhesives*, vol. 23, pp. 215-223, 2003.
- [18] M. Lucic, A. Stoic e J. Kopac, «Investigation of aluminum single lap adhesively bonded joints,» in *International scientific conference on contemporary achievements in mechanics, manufacturing and material science*, Gliwice-Zakopane, Poland, 2005.
- [19] C. Borsellino, G. Di Bella e V. F. Ruisi, «Adhesive joining of aluminium AA6082: The effects of resin,» *International Journal of Adhesion and Adhesives*, vol. 29, pp. 36-44, 2009.
- [20] G. Critchlow e D. Brewis, «Influence of surface macroroughness on the durability of epoxide-aluminium joints,» *International Journal of Adhesion and Adhesives*, vol. 15, pp. 173-176, 1995.

- [21] J. Ferreira, P. Reis, J. Costa e M. Richardson, «Fatigue behavior of composite adhesive lap joints,» *Composites Science and Technology*, vol. 62, pp. 1373-1379, 2002.
- [22] S. Krenk, J. Jonsson e L. P. Hansen, «Fatigue analysis and testing of adhesive joints,» *Engineering fracture mechanics*, vol. 53, pp. 859-872, 1996.
- [23] O. C. Zienkiewicz, G. C. Nayak e D. J. R. O, «Composite and "overlay" models in numerical analysis,» *Foundations of plasticity*, pp. 107-122, 1972.
- [24] M. Quaresimin e M. Ricotta, «Fatigue behaviour and damage evolution of single lap bonded joints in composite material,» *Composites science and technology*, vol. 66, pp. 176-187, 2006.
- [25] A. Pirondi e F. Moroni, «An investigation of fatigue failure prediction of adhesively bonded metal/metal joints,» *International Journal of Adhesion & Adhesives*, vol. 29, pp. 796-805, 2009.
- [26] S. Hurme e G. Marquis, «Shear fatigue of the bonded and frictional interface under constant normal pre-stress,» *International Journal of Fatigue*, vol. 70, pp. 1-12, 2015.
- [27] *User guide Wyko NT1100 surface profiler.*
- [28] D. Kopeliovich, «Substances&Technology,» 2012. [Online]. Available:
http://www.substech.com/dokuwiki/doku.php?id=adhesive_joints.
- [29] AZoM, «AZO materials,» 2013. [Online]. Available:
<https://www.azom.com/article.aspx?ArticleID=8621>.
- [30] AZoM, «AZO materials,» 2006. [Online]. Available:
<https://www.azom.com/article.aspx?ArticleID=3328>.